# Enhancing 3D Printed Substrates Using Atomic Layer Deposition

by

**Atilla C. Varga**

A thesis submitted to the Faculty of Graduate and Postdoctoral Affairs in partial fulfillment of the requirements for the degree of

Master of Science

In

Chemistry

Carleton University
Ottawa, Ontario

*This thesis is dedicated to my family*

# Abstract

This thesis outlines the integration of 3D printing and Atomic Layer Deposition (ALD) to create advanced 3D printed architectures. Polymer nanocomposite materials have been synthesized using common polymer materials to alter physical properties however these nanocomposites are synthesized prior to use. In this thesis, Atomic Layer Deposition (ALD) was used in combination with common and inexpensive polymer materials post model creation (using 3D printing) to create nanoscale hybrid materials. 3D printed Acrylonitrile Butadiene Styrene (ABS) and Polyvinyl Alcohol (PVA) polymer structures were coated and infiltrated with alumina ($Al_2O_3$) using the trimethylaluminum(III) (TMA) and water ALD process. Coating studies on ABS were carried out at 80 ˚C, which resulted in a 203 nm thin film with a 1.35 Å growth per cycle (GPC). The thin film was a well-adhered protective overcoating on ABS which prevented the reaction with acetone vapors in a solvent resistance experiment. Scratch and more aggressive tape tests were not able to remove the overcoating completely from the polymer surface which provided a 50 % and 32 % increase in acetone vapour resistance before initial deformation and complete structure collapse respectively. Infiltration studies on ABS and PVA structures were preformed at 130 ˚C and 80 ˚C respectively, to alter their physical properties. Differential Scanning Calorimetry (DSC) was used to determine the Glass Transition Temperature ($T_g$) of the polymers pre- and post-deposition after varying the number of ALD cycles, resulting in a change of ~ 9 ˚C and ~ 27 ˚C for ABS and PVA, respectively. After one heat cycle the post-deposition $T_g$ reverted back to its pre-disposition point indicating reversibility of the deposition effects are possible. Optimal growing patterns, polymer composition, and inhibiting surface coatings were examined by Energy Dispersive X-ray Spectroscopy (EDS) mappings which effected the amount of infiltration possible within the polymer substrate and in turn $T_g$. These results achieved provides guidelines to creating nanoscale hybrid materials using 3D printing and ALD via coating and infiltration and in tern altering the physical and thermal properties of 3D printed polymer architectures with significant impact in the development of advanced 3D printed architectures leading to a wide array of applications in polymer and material chemistry.

# Preface

This preface provides full bibliographical details for each article included in this thesis, as well as whether the article is reproduced in whole or in part. Use of copyrighted material is likewise acknowledged here. When citing material from this thesis, please cite the article relevant to the chapter if the chapter is based on a publication. All published Supplementary Information is freely available via the Internet.

Pursuant to the Integrated Thesis policy of Carleton University, the supervisor (Seán T. Barry) and the "student" (Atilla C. Varga) confirm that the student was fully involved in setting up and conducting the research, obtaining data, and analyzing results, as well as preparing and writing the material presented in the co-authored article(s) integrated in the thesis. Additionally, the supervisor confirms the information provided by the student in this preface.

# Chapter 2

Atilla C. Varga and Seán T Barry. Modified 3D-Printed Architectures: Effects of Coating by Alumina on ABS. *J. Vac. Sci. Technol. A* **40**, 022407. **2022.** Copyright 2022 AVS (Science and Technology of Materials, Interfaces, and Processing).

This publication is wholly reproduced and edited for formatting and clarity of presentation. Atilla C. Varga designed and carried out the experiments along with thermogravimetric analysis. SEM and EDS analysis were performed by Atilla C. Varga with the help of SEM microscopist Dr. Jianqun Wang (Carleton University). The publication was written by Atilla C. Varga.

# Chapter 3

Atilla C. Varga and Seán T Barry. Reversable Alteration of 3D Printed Polymer Properties via Infiltration of Alumina by Atomic Layer Deposition. *Submitted.*

This manuscript is wholly reproduced and edited for formatting and clarity of presentation. Atilla C. Varga designed and carried out the experiments along with thermogravimetric analysis. SEM and EDS analysis were performed by Atilla C. Varga with the help of SEM microscopist Dr. Jianqun Wang (Carleton University). The publication was written by Atilla C. Varga.

# Acknowledgements

I would like to thank everyone who has helped me throughout the years and in accomplishing this thesis. From Prof. Seán T Barry for letting me have this amazing opportunity to be apart of the Barry Lab and guidance throughout. To all the amazing people in the Barry lab and especially Dr. Matthew Griffiths who has taught me from when I was an undergraduate student all the synthetic chemistry skills and passed on so much of his great knowledge to me. Dr. Goran Bačić who has always offered help and guidance from when I first join the lab and Dr. Peter Gordon who showed me how to operate and use the many of ALD tools at Carleton. To all the other Barry lab members, thank you for your constructive comments, suggestions, and guidance throughout my research project.

All of the amazing staff at Carleton University from Prof. Robert Burk who made chemistry so fun and exciting in first year that I decided to switch into chemistry. The amazing professors where I learned a lot about different fields, the laboratory coordinators who helped teach and improve many laboratory techniques and the administrative staff for helping with many program requirements, deadlines, and applications. Special thanks is also given to Dr. Jianqun Wang who taught me how to operate a SEM and EDS which was used very often throughout this thesis.

My family deserves many thanks as this could not have been done without their support and love, my parents Romy and Krista have always encouraged and helped me to strive to be the best I can be along with a few kicks in the rear when they knew I could do better.

Finally, my amazing wife Ksenia who is always by my side and supports me throughout the tough times to help accomplish all that I have. Your drive for excellence motivates me to do the same and your endless love plus support is all that one could need, I love you!

Thank you all!

# Contents

# List of Figures

# List of Tables

# Abbreviations

| | |
|---|---|
| **3D** | Three Dimensional |
| **ABS** | Acrylonitrile Butadiene Styrene |
| **ALD** | Atomic Layer Deposition |
| **ASA** | Acrylic Styrene Acrylonitrile |
| **CFC** | Carbon Fiber Composite |
| **DLP** | Digital Light Processing |
| **DSC** | Differential Scanning Calorimetry |
| **EDS** | Energy Dispersion X-Ray Spectroscopy |
| **FC** | Fiber Composite |
| **FDM** | Fused Deposited Modeling |
| **FFF** | Fused Filament Fabrication |
| **GPC** | Growth Per Cycle |
| **HIPS** | High Impact Polystyrene |
| **MC** | Metal Composite |
| **Nylon** | Polyamide |
| **PC** | Polycarbonate |
| **PEEK** | Polyetheretherketone |
| **PETG** | Polyethylene Terephthalate Glycol |
| **PLA** | Polylactic Acid |
| **PLA+** | Polylactic Acid - Annealed + Additives |
| **PP** | Polypropylene |
| **PVA** | Polyvinyl Alcohol |
| **PwC** | Powder Composite |
| **SCCM** | Standard Cubic Centimeter per Minute |
| **SEM** | Scanning Electron Microscopy |
| **SLA** | Stereolithography |
| **$T_g$** | Glass Transition Temperature |

| | |
|---|---|
| **TGA** | Thermal Gravimetric Analysis |
| **TMA** | Trimethylaluminum |
| **TPE** | Thermoplastic Elastomers |
| **TPU** | Thermoplastic Polyurethane |
| **UV** | Ultraviolet |

# Chapter 1

# Introduction

## 1.1 Motivation

In recent years 3D printing has gained enormous popularity thanks to its affordability, accessibility, ease of use, and the ability to easily employ a variety of polymer materials.[1] These polymer materials offer a variety of options regarding various properties such as flexibility, durability, and strength, which make them the ideal for 3D printing filaments in addition to the ability to incorporate metal powders, fibers, etc. to create composite materials. However, many of these more exotic and extreme polymer materials are expensive and require speciality equipment to print: most common 3D printers are limited to lower printing temperatures and use of safe materials.[2–4]

Polymer nanocomposite materials have been synthesized using common polymer materials and various metals/oxides to show the alteration of polymers physical properties[5–7] and provide protective surface coating.[8–10] These nanocomposite materials have increased temperature resistance, durability, and solvent resistance. However, they are synthesized prior to use (either synthesized in bulk or simultaneously during polymerization) making it not ideal to be used in a 3D printer for model creation. Atomic Layer Deposition (ALD) has been used in combination with polymer materials to create nanoscale hybrid materials post model formation.[11–16] These include the addition of various metals and/or oxides through infiltration into polymer materials which react with the polymer structures to enable polymer functionalization, nanoparticle growth, and altered polymer properties. As such the materials have been employed in catalysis, as extreme chemical resistance polymer materials and conductive polymers.

Hence the integration of 3D printing and industrial nanoscale processes such as ALD will have a significant impact in the development of advanced 3D printed architectures leading to a wide array of applications. ALD modification of 3D printed structure can be applied in nanoparticle growth, which has applications in low-cost high surface area catalysts. Both

thin film coatings as well as precursor infiltration can have applications in chemical resistant polymer coatings, conductive polymer networks, and various other applications of interest in electronics, sustainable materials, and manufactured products. More specifically, our lab uses 3D printed parts in ALD reactors as substrate holders and various devices in the reaction chamber. The thermal and chemical limits of the 3D printed architectures limits the deposition conditions by the polymer's properties, for example the deposition temperature, use of plasma and type of precursors used which could all damage the 3D printed part. Hence the modification of 3D printed architectures using ALD to either provide a protective coating or to modify polymer properties (via infiltration) will enable and expand the range of deposition conditions and process parameters where these parts can be employed. Thus, being able to control preferential coating or infiltration will allow for specified and optimized applications for of each a protective coating or modified polymer properties respectively.

## 1.2 Atomic Layer Deposition

Atomic layer deposition (ALD) is a layer-by-layer, thin film deposition technique which has a primary use of creating thin film coatings for applications ranging from batteries, to solar cells, and most notably in creating semiconductors.[17,18] There are also numerous less investigated applications ranging in pharmaceuticals and catalysis, to name a few examples.[16,19–21] ALD onto polymers has gained significant interest within the materials chemistry field due to large number of applications such as nanoscale templates, surface modification layers, barrier coatings, and area selectivity.[11,13,21] The majority of these applications and techniques take advantage of ALD's selectivity and very good conformality on high aspect ratio features.[22] Other thin film deposition techniques are unable to achieve the same conformality as ALD, since ALD uses self-limiting surface reactions. Self-limiting surface reactions occur when the compound will only react with the substrate it is being deposited onto and not itself to create a monolayer across the entire surface.[23] This enables conformal coverage of the entire substrates surface (including features such as stands/wires, trenches, peaks, etc.) and is not affected by line of sight like other deposition techniques.[24]

The process for depositing thin film by ALD is to sequentially expose the surface through a series of pulses with a precursor to create a monolayer and then co-reagent to alter the composition of the deposited monolayer which is then reactivated for further growth. A schematic of this sequential process is shown in Figure 1.1, where the blue/orange spheres represent the precursor, and the red spheres represent the co-reagent which reacts at the surface to alter the chemical composition of the precursor to enable further deposition. Purge steps are used to clear the deposition area of any unreacted precursor or co-reagents.

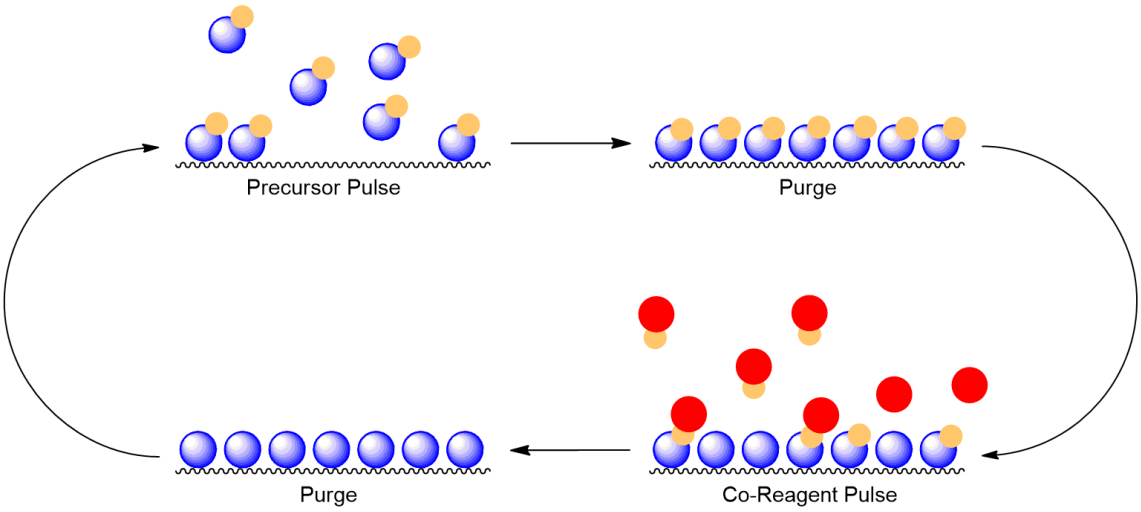


**Figure 1.1** ALD layer-by-layer growth scheme. Precursor pulse introduces the main precursor to the surface where it reacts to create a monolayer, followed by a purge step to remove any excess precursor. The co-reagent is then pulsed to modify the surface species and/or add secondary elements (such as oxygen or nitrogen), again followed by a purge step. Process is then repeated to get a desired film thickness.

The ALD sequential process from Figure 1.1 can be repeated several times to create a film with the desired thickness. For ALD applications which require an oxide or nitride thin film, the co-reagent is commonly the oxygen or nitrogen source. Then the sequential process is repeated in the same manner to create alternating metal-oxygen or metal-nitrogen layers which make up the thin film.[25] This process is shown in Figure 1.3 for the ALD process employed in this thesis.

### 1.2.1 Growth Characteristics

As previously noted, ALD is a self-limiting, saturative thin film deposition technique which means that during each precursor pulse the amount of precursor which reacts with the surface is determined and limited by a finite number of available surface binding sites. Once the precursor has been chemisorbed to the surface and once all surface sites are occupied, any additional precursor should not react with itself, and no further deposition will occur.[26] This can be visualized by using a saturation curve shown in Figure 1.2(a), where the mass gain per ALD cycle is plotted against the pulse time of the precursor. As additional precursor is exposed to the surface and surface sites are occupied, film growth beings to plateau and then stops altogether.

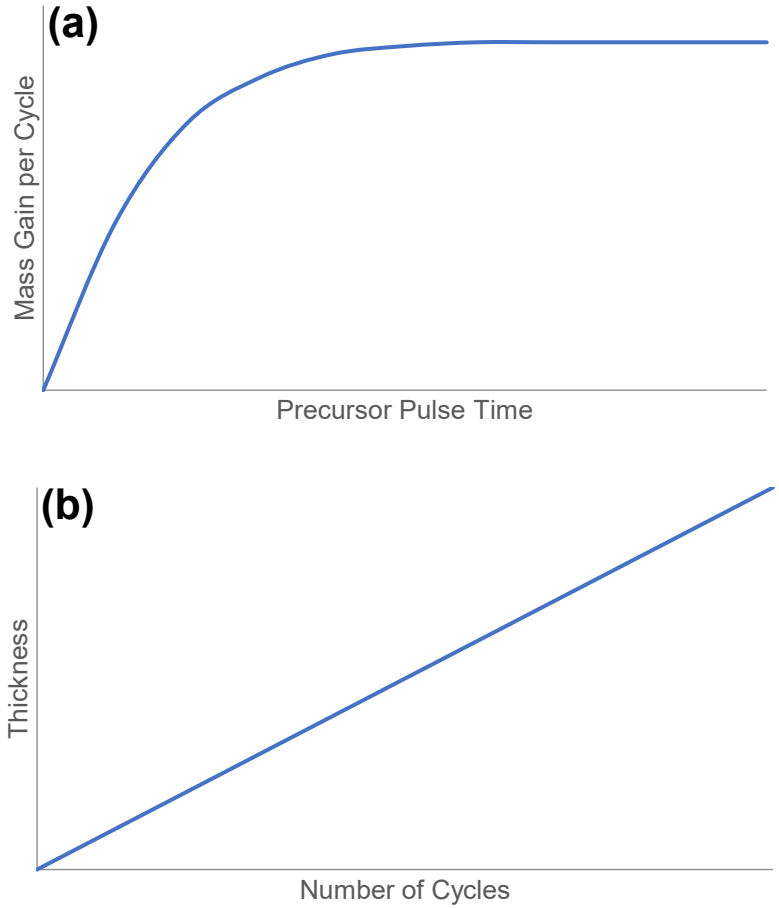


**Figure 1.2** Optimal ALD precursor and growth characteristics with (a) showing precursor surface saturation behaviour and (b) showing GPC linear behaviour.

The same phenomenon can be observed in a larger scope for the repeated cyclic ALD process. Since each precursor pulse will behave in the same manner, one additional monolayer (which has an associated thickness increase) will be deposited during each cycle. Hence the overall film thickness in relation to the number of cycles can be observed in Figure 1.2(b) which results in a linear growth per cycle (GPC) behaviour. The resulting linear relationship is very useful and desirable for thin film synthesis since atomic layer control (at an Angstrom level) can be achieved by altering the number of ALD cycles which directly corresponds to a known number of monolayers and in turn, thickness.[27]

Very selective, calculatable, and predictable growth characteristics make ALD the ideal technique for creating nano scale thin films and additionally have very conformal coverage of polymer substrate materials.

### 1.2.2 Precursor Design

An ALD precursor is the chemical compound (reactant) which is used for delivering the desired element to the surface or substrate for deposition. The precursor reacts with the surface by first physisorbing and then chemisorbing to create a surface bond. There are different physical and chemical properties which determine the usefulness of a precursor as well as how it will behave with a given substrate which will be briefly discussed in this section.

ALD precursors come in a wide range of types with different metals, heteroatoms (e.g., oxygen, nitrogen, silicon, etc.) and complexities (e.g., monomers, dimers, trimers, chelates). The commonality between ALD precursors are a few key factors which need to be met: volatility, thermal stability and a self-limiting growth behaviour. The self-limiting behaviour is common for all ALD precursors where additional precursor should not be able to bind to itself once deposited onto a surface. Volatility and thermal stability of precursors can be widely different depending on the desired process and in turn, use. In brief, given said process conditions the precursor needs to volatile with a large enough vapour pressure for delivery into the reaction chamber while not undergoing decomposition. For example, if a certain precursor will be used to deposit gold onto an organic substrate, the deposition temperature needs to be below the temperature at which the organic substrate beings to

decay or degrade. Hence such a precursor needs to have a low volatility for deposition onto the organic substrate. If the same precursor was used instead in a process where the deposition needed to be carried out at 300 ˚C, the decomposition point of the precursor would have to be above 300 ˚C, otherwise the precursors would decompose and no ALD would occur.

For the purpose of this thesis, an existing well studied precursor which can be deposited at low temperatures and has a high decomposition point was chosen. Since this would allow for a large range of deposition temperatures, it would also accommodate for all 3D printing polymers to be used as the substrate. Hence, an aluminum oxide (alumina) thin film process was employed using Trimethylaluminum(III) (TMA) as the primary precursor and water as the oxygen precursor.[28] Due to the favourable volatility, thermal stability and extensive literature background, TMA and water has been used to deposition alumina at temperatures ranging from as low as 33 ˚C to above 300 ˚C.[29] The cyclic growth pattern for TMA and water follows the general growth outlined in Figure 1.1 with the specific process shown in Figure 1.3 below.

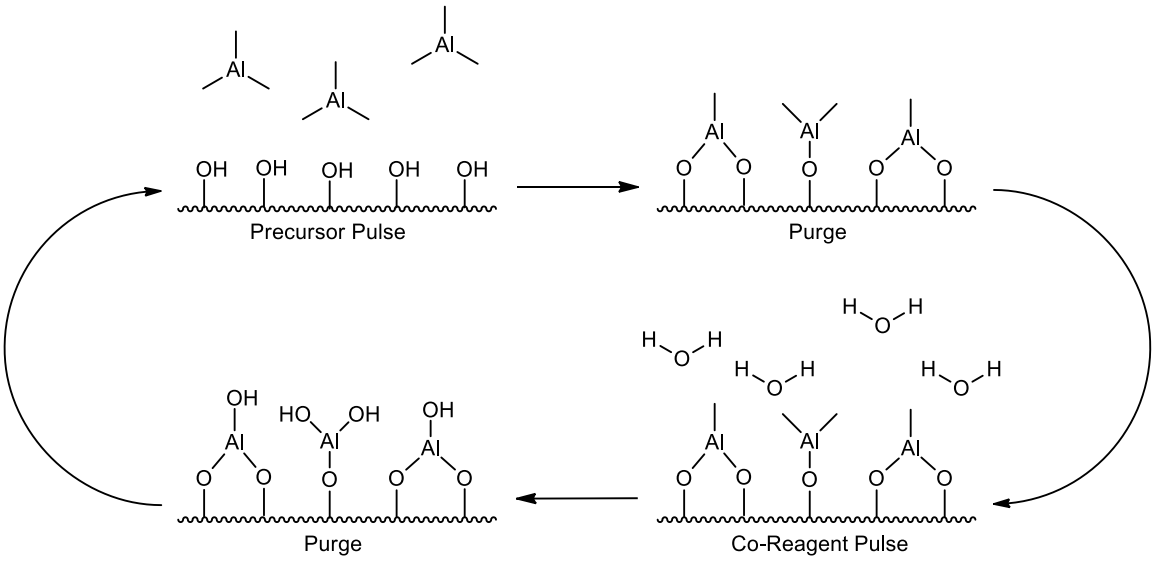


**Figure 1.3** ALD layer-by-layer growth scheme for TMA and water process. The co-reagent being water is used as the oxygen source as well as to modify the TMA surface species to create hydroxyl functional groups for further deposition.

### 1.2.3 Infiltration

So far, the aspects of ALD have been discussed with respect to a surface coating on a given substrate. Another possibility during deposition is to have infiltration of the precursors into the bulk material where the precursors then react within the substrate and in turn deposit the target material. For this to be a possibility the substrate has to be porous enough to allow sufficient diffusion of the precursors into the substrate. In the case of polymers, the spacing between polymer strands dictates how much room the precursors have to diffuse into the bulk material. In the majority of cases, the spacing between strands is large enough to allow for precursor diffusion into the bulk and for optimal infiltration it is more critical to choose a polymer based on chemical composition and properties which work with the target process.[30] What determines the spacing size of the polymer strands will be discussed in a further section. As for 3D printed polymers, the process of infiltration is slightly different which can be seen in Figure 1.4 below.

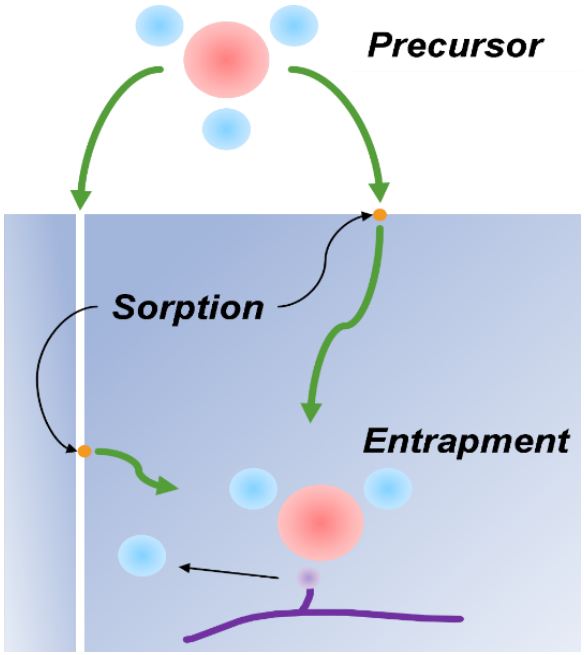


**Figure 1.4** Precursor infiltration in a 3D printed polymer. Precursors in vapour phase first enters the bulk polymer material at sorption points (shown by orange dot on the surface of blue bulk material) either on the surface or between 3D printed layers. Precursor then diffuses through the bulk until it reacts and binds with the polymer to become entrapped. Adapted from *Leng C. and Losego M.*[30]

For a traditional infiltration process the bulk material is considered to be uniform and completely connected. As for a 3D printed polymer, due to the nature of how the structures are created (which is outlined in the following section) there are a series of touching layers. Hence a 3D printed structure can be considered as layers of bulk material and in between each of these layers there is enough space for a precursor in the vapour phase to diffuse into. Then as seen from Figure 1.4, the sorption site at which the precursor enters the polymer bulk can not only be at the surface but further into one of these layer spacings. This results in an infiltration gradient which is not only present from the surface down into the bulk but also from each layer spacing diagonally which results in a gradient shown in blue from Figure 1.4. Hence more infiltration would also be possible since the exposed surface area (or aera which can be exposed to gaseous precursor) is much larger than for traditional very uniform bulk substrates which only have the top and side surfaces exposed to precursor.

## 1.3 3D Printing

3D Printing or additive manufacturing is a layer-by-layer process used to create 3D objects from a material source. There are two main modes of 3D printing; material extrusion and vat polymerization.[31–33] The latter involves a vat of liquid resin which is hardened one layer at a time using a light source (often UV). Common forms of vat polymerization 3D printing are Stereolithography (SLA) and Digital Light Processing (DLP).[34] The second and more common mode of material extrusion, uses a material source which is often spools of filament which are extruded through a heated nozzle as shown by Figure 1.5. This method of material extrusion is called Fused Deposited Modeling (FDM) or Fused Filament Fabrication (FFF) and is among the most common for hobbyists, researchers, and industry alike due to its affordability, speed, size variability, and ease of use.[35–40]

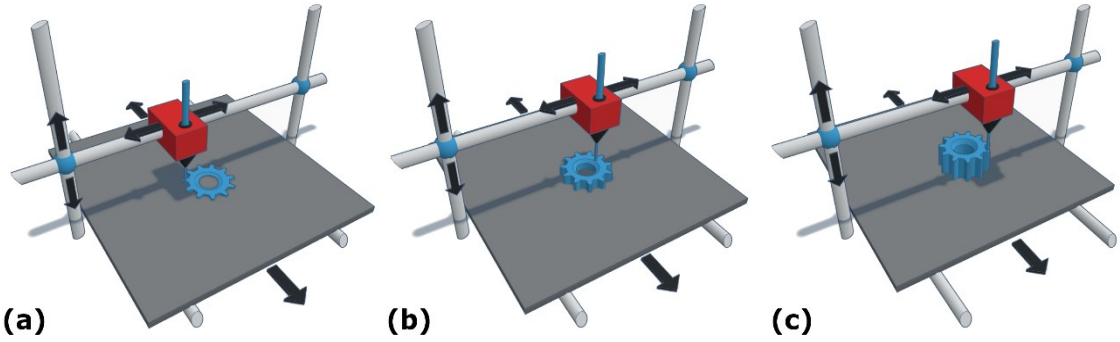


**Figure 1.5** Schematic diagram of a FDM 3D printer. Black arrows indicate how the printer moves in three dimensions along each of the axis. Red rectangle represents the printer head with the black cone showing the heated hot end and nozzle tip. Silver rods are used to slide printer head along 3 axis using ball bearings. (a-c) represents the progression of printing layer-by-layer to build up the desired model.

In FDM 3D printing (which is used in this work), a filament is loaded into the printer head where a set of sprockets pinch the filament to control the movement and extrusion speed of the filament. As the filament is pushed through the printer head it begins to be heated by the hot end, which is set to a specific temperature based on the material being used. The filament is heated just enough to be soft and malleable but not a liquid. The material is then extruded through a small nozzle within a millimetre of the printer bed or already deposited material to ensure proper bonding. As the printer head moves continuously from one location to another, the deposited material beings to cool and solidify bonding to the layer underneath. This process is continuously repeated in a layer-by-layer upward (z-axis) direction with each x-y layer formed following a pattern, determined from a 3D model using a "slicing" software. For models which have overhanging or steeper than 45˚ angle features, support material must be used as a scaffolding structure: this is then easily removed once the print is complete.

There is a range of different materials which can be used in FDM 3D printers: polymers, metals, organic tissues, concrete, clay/ceramic, fibers (such as glass fiber, carbon fiber, etc.), and composite materials. Not every FDM 3D printer will be able to print using the above-mentioned materials since some require specialty components. For example, metal 3D printers need to have a printer head and hot end which can withstand the higher

temperatures required to soften various metals for printing. Hence the most common and accessible FDM 3D printers (as the one using for this work) are limited to using polymers, and polymer composite materials. This still encompasses a large range of options.

### 1.3.1 3D Printing Polymers

The number of available polymers for 3D printing use has grown due to the increase in popularity. Additionally, the most common FDM 3D printers are limited to polymers and polymer composites due to their lower printing temperatures required. This allows for cost effective parts to be used in printer assembly and the absence of a need for liquid cooling. Despite that material limitation, the number and wide range of polymers which can be used is shown below.

**Table 1.1** FDM 3D printing polymer materials with category separation and extrusion temperature needed for printing.[41–43]

| Type | Abbreviation | Material Description | Extrusion Temp /°C |
|---|---|---|---|
| Standard | PLA | Polylactic Acid | 215 |
| | PLA+ | Polylactic Acid - Annealed + Additives | 230 |
| | ABS | Acrylonitrile Butadiene Styrene | 255 |
| | PETG | Polyethylene Terephthalate Glycol | 230 |
| Less Common | Nylon | Polyamide | 250 |
| | PC | Polycarbonate | 275 |
| | ASA | Acrylic Styrene Acrylonitrile | 260 |
| | PEEK | Polyetheretherketone | 360 |
| | PP | Polypropylene | 220 |
| Flexible | TPU | Thermoplastic Polyurethane | 230 |
| | TPE | Thermoplastic Elastomers | 230 |
| Water Soluble | PVA | Polyvinyl Alcohol | 195 |
| | HIPS | High Impact Polystyrene | 220 |
| Composites | CFC | Carbon Fiber Composite | 265 |
| | MC | Metal Composite (e.g., Alumide) | 275 |
| | FC | Fiber Composite (Glass, Kevlar, etc.) | 260 |
| | PwC | Powder Composite (Wood, Chalk, etc.) | 190 |

As seen from Table 1.1, the large variety of useable polymers yields many different types (such as hard, flexible, water soluble, etc.) in addition to each polymer having unique

physical properties. These properties encompass various uses: more resistant to temperature, bending, have better durability, etc. In addition, the ease of printing or printability of the various polymers is influenced by these properties. For example, if you were to compare the two most common polymers ABS and PLA, both are a hard plastic when printed. However, ABS has better durability, strength, and is more resistant to increased temperature. As such it requires a higher printing temperature (as seen in Table 1.1) which when cooling can lead to the model warping, making the printability lower than for PLA. These factors can make some of the more exotic and special case polymers much more difficult and expensive to print, which puts them out of reach for common FDM 3D printers. However much like the composite materials which take advantage of the common and easy to use polymers combined with specialty materials yields a good quality, easily accessible and low-cost hybrid material. This same philosophy had been applied in this thesis to combining ALD with commonly used polymers to create advance 3D printed architectures. Specifically, ABS and PVA were used whose structures are sown in Figure 1.6 below.

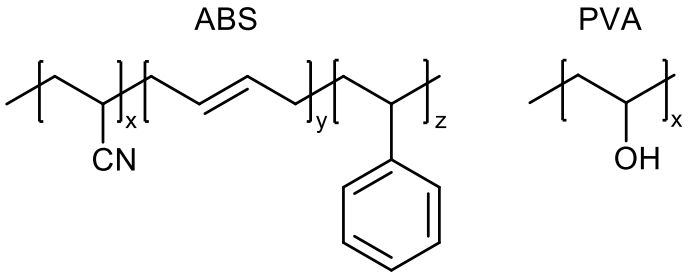


**Figure 1.6** Chemical structure of ABS and PVA polymer chains. Where for ABS x, y and z represent the varying number of acrylonitrile, butadiene and styrene functional groups present in the polymer chain respectively. As for PVA, x represents the number of hydroxyl functional groups.

The rationale for choosing ABS and PVA polymer materials are due to practical uses and theoretical hypothesise. As mentioned previously, in the Barry Lab ABS 3D printed architectures were being used in ALD reactors due to the higher temperature resistance compared to other common filaments. As such the use of ABS in further experiments was

beneficial and practical as there would be an immediate use and application within the lab. For PVA, this 3D printing polymer was chosen as a theoretically highly reactive polymer to the TMA and water process for infiltration. TMA can be described as a Lewis acidic molecule since it has an empty p-orbital which is capable of accepting electron density usually in the form of a lone pair form a Lewis base (such as from the oxygen lone pair in the case of a TMA and water process).[22] Hence, PVA would be an ideal candidate for optimal reactivity and infiltration since it possesses hydroxyl functional groups which are perfect for TMA binding. In addition, TMA can also interact with other high electron density sites such as the cyano, olefin and styrene found in ABS by overlapping the empty p-orbital with the areas of high electron density.[11] This is how TMA can interact and be deposited on ABS but as will be discussed in subsequent chapters, TMA will preferentially interact and therefore grow aluminum oxide in more favourable conditions.

### 1.3.2 Glass Transition Temperature ($T_g$)

There are many factors which effect the physical properties of a polymer along with the polymer strand spacing which can be described in short by the chemical composition of the monomer(s) comprising it, the secondary and tertiary structures (i.e., stereochemistry of the polymer strand linkages, intermolecular interactions, chain length and distribution).[44] One such properties is the glass transition temperature ($T_g$) which occurs in amorphous materials and is the temperature at which the polymer goes from a glassy (hard and brittle) state to a rubbery (soft and malleable) state or vice-versa.[44,45] This transition is not an immediate transition but rather a gradual change moving from one state to another. The $T_g$ is very useful in polymer science since it can be used in determining a working range for many polymers as well as being directly related to the materials strength and capabilities: this is all useful information for appropriate applications.[42,43] For hard plastics such as ABS, PLA, PETG, etc. the polymers are used and implemented well below the $T_g$ in their glassy state to ensure a rigid and strong material where as TPU and TPE are used above their $T_g$ since they are flexible materials used in their rubbery state.

As mentioned above the $T_g$ of a polymer is affected by the polymer's inherent chemistry, which means mechanical mixtures of multiple polymers or composite materials will have

little to no effect on the $T_g$ of a polymer.[44] Chemical alterations of the polymer structure however can yield to an altered $T_g$ and have been shown through surface modification,[46] functionalization,[7–9,47,48] and nanocomposite formation.[5,6,10,48–51] Hence the $T_g$ of a polymer is an important property to consider for intended applications and the effects of deposition via ALD on the $T_g$ of various polymers could have a significant impact.

### 1.3.3 Differential Scanning Calorimetry (DSC)

Differential Scanning Calorimetry (DSC) is a calorimetric technique (measurement of heat by analysing the heat exchange between two samples)[52] which is used to measure the heat flow difference between a sample and a reference. The heat flow difference will result in exothermal (heat released by the sample) and endothermal (heat adsorbed by the sample) events which can be used to determine phase changes. DSC can also be used to measure the $T_g$ of a polymer by observing the step change or the inflection point in a DSC trace.[53,54]

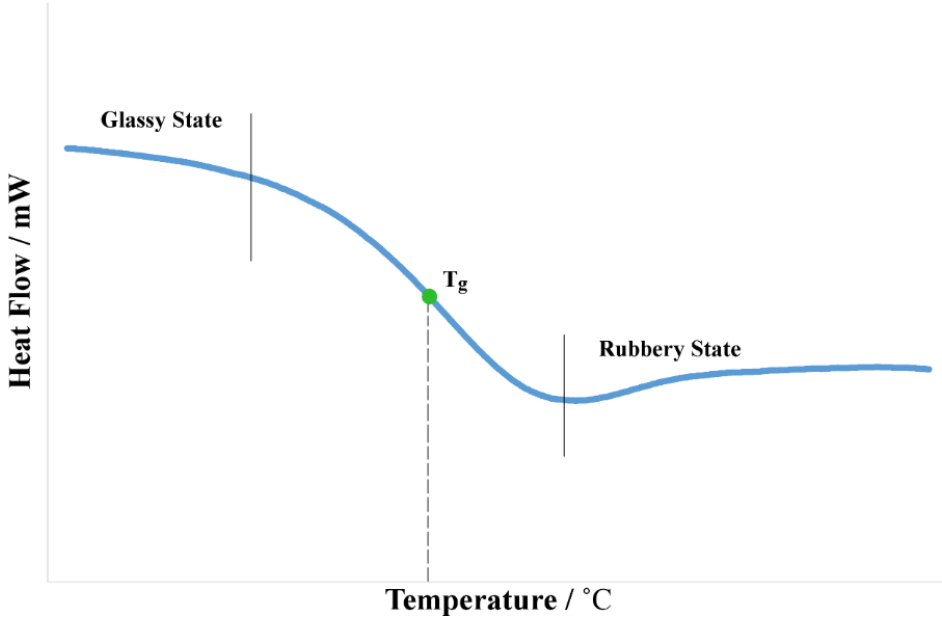


**Figure 1.7** DSC trace of PVA polymer with $T_g$ point shown by green dot (50 ˚C), glassy and rubbery states shown above and below the $T_g$ respectively.

As seen from Figure 1.7 the typical $T_g$ of a polymer is found within a step change of the DSC trace. As mentioned previously this change is a gradual shift from one state to another

and hence the $T_g$ of a given material is taken at approximately the midpoint of this transition. The specific value of this midpoint and therefore $T_g$ can be calculated either by determining the inflection point between the concave down and up sections or by using the tangent point of intersecting constructed parallel lines to the glassy and rubbery state regions.[55] The former is the more accurate, consistent, and the preferred method for $T_g$ determination using DSC due to ease of definition and limited error.[56]

# Chapter 2

# Modified 3D-Printed Architectures: Effects of Coating by Alumina on ABS

*Reprinted and adapted from the original article published as:*

Atilla C. Varga[a] and Seán T Barry.[a] Modified 3D-Printed Architectures: Effects of Coating by Alumina on ABS. *J. Vac. Sci. Technol. A* **40**, 022407. **2022.** 

[a] Department of Chemistry, Carleton University, 1125 Colonel By Drive, Ottawa, Ontario, K1S 5B6, Canada

# Abstract

3D-printed acrylonitrile butadiene styrene (ABS) polymer structures were coated with alumina ($Al_2O_3$) using the trimethylaluminum(III) (TMA) and water ALD process at 80 ˚C, which resulted in a 203 nm thin film with a 1.35 Å growth per cycle (GPC). This thin film was a well-adhered protective overcoating on ABS to prevent reaction with acetone vapors in a solvent resistance experiment. Scratch tests were not able to remove the overcoating from the polymer surface which provided a 50 % and 32 % increase in acetone vapour resistance before initial deformation and complete structure collapse respectively. A more aggressive tape test did cause delamination of the protective coating. This proof-of-concept experiment demonstrates how 3D-printing combined with ALD overcoating can alter the chemical characteristics of complex polymer architectures.

## 2.1 Introduction

Additive manufacturing – including 3D printing – is a common and inexpensive technique due to the large variety of accessible and printable polymers.[43] The majority of materials used in 3D printing are comprised of organic polymeric structures that degrade when exposed to different conditions or chemicals (Table 2.1).[34] Among the polymers typically used in 3D printing, acrylonitrile butadiene styrene (ABS) is the second most commonly used filament due to its low cost, high durability, tensile strength and stiffness, wide temperature range and impact resistance.[57]

**Table 2.1** 3D printing materials in descending order of commonality.[58] PLA (Polylactic Acid), PETG (Glycol modified Polyethylene Terephthalate), PC (Polycarbonate) and TPU (Thermoplastic Polyurethane). Maximum working conditions of polymers are below the Glass Transition Temperature ($T_g$). Prices are in USD for 1kg filament spools from Amazon as of September 2021.

| Material | PLA | ABS | PETG | TPU | PC |
|---|---|---|---|---|---|
| Price / Kg | 10-40 | 10-40 | 20-60 | 30-70 | 40-75 |
| Soluble | Acetonitrile | Acetone | THF | THF | Chloroform |
| $T_g$ / ˚C | 60 | 105 | 81 | 60 | 147 |

Atomic layer deposition (ALD) is a layer-by-layer thin film deposition process[59] which can be used to deposit many different materials on different polymer substrates.[9,12,21] This can be combined with 3D-printed polymer structures to alter the inherent processing characteristics of the polymer substructure by depositing a thin surface coating. Herein, we report on our investigation of 3D-printed ABS substrates both above and below the glass transition temperature ($T_g$ = 105 ˚C[60]) of the polymer with an overcoating of $Al_2O_3$ ALD using trimethylaluminum(III) (TMA) and water. This is the prototypical ALD target film using well-defined precursors, and both the deposition and the film characteristics of this process have been investigated thoroughly on a variety of substrates.[61] The deposition can be performed over a wide temperature range, from 33 ˚C to around 300 ˚C, as a thermal

process, which eliminates the concern of plasma treatment damaging the integrity of a 3D-printed structure during the deposition process.

## 2.2 Experimental

Unless otherwise noted, all reagents were purchased from commercially available sources and used as received (Sigma Aldrich and Strem Chemicals). 3D-printed structures were supplied by Kromati.ca using a white ABS polymer (Prusament ABS). ABS structures were printed in an enclosure using 100 ˚C heated bed temperature and 255 ˚C nozzle temperature.

ALD experiments were carried out using a Picosun R-200 Standard ALD tool. Depositions were carried out using Trimethylaluminum (97 %, Aldrich), $H_2O$ (HPLC grade, Aldrich), and a carrier gas of Nitrogen (>99.9999 %, Praxair). Process parameters included an intermediate space of 600 SCCM, stabilization time of 60 s, and flow rate of 150 SCCM and 200 SCCM for TMA and $H_2O$ respectively.

Individual deposition process parameters were as follows:

**Table 2.2** List of ALD coating recipes with process parameters.

| Run | TMA | | $H_2O$ | | Temperature / ˚C | Cycles |
|---|---|---|---|---|---|---|
| | Pulse / s | Purge / s | Pulse / s | Purge / s | | |
| ABS-1 | 0.1 | 20.0 | 0.1 | 40.0 | 120.0 | 1500 |
| ABS-5 | 0.1 | 20.0 | 0.1 | 40.0 | 80.0 | 1500 |
| ABS-B1 | 0.1 | 20.0 | 0.1 | 40.0 | 80.0 | 1500 |

ABS-B1 is denoted as a separate ALD recipe since the chamber conditions were different than ABS-5 (which has the same pulse program). To accommodate for the larger size of the 3D-printed Benchy (a common 3D printing object used for testing and calibration), the reactor stage was removed, and the sample was placed on a metal plate at the bottom of the reaction chamber. GPC and thickness for ABS-5 was determined by using a reference Si

wafer and obtained k-rations from EDS which were imputed into BadgerFilm plus the density of alumina thin film,[61] to result in calculated film thicknesses and hence GPC.

Sample preparation for SEM and EDS analysis involved coating the alumina coated ABS structures with a layer of carbon film. This was done using a Quorum Q150T ES sputter/evaporator tool by evaporating a carbon layer using graphite. SEM imaging was preformed using a Tescan Vega-II XMU VPSSEM tool in both secondary electron and backscatter electron imaging modes with a working distance of ~ 10 nm and accelerating voltage of 10 kV for all scans. EDS data collection was preformed in conjunction with SEM imaging using an Oxford Instruments Inca EDS tool.

## 2.3 Results and Discussion

The surfaces of 3D-printed ABS objects show natural ridges as individual extrusion lines (~0.15 mm across), which are formed during printing (Figure 2.1a). Annealing of the ABS substrate below 105 °C (i.e., the $T_g$ of ABS) alters the surface a minor amount, but the ridged morphology remains intact (Figure 2.1b). Annealing the ABS at 130 °C removes the ridges but there remains striation due to the printing and the overall printed structure remains in tact (Figure 2.1c), while annealing at 150 °C almost fully removes these surface features, with the overall 3D-printed structure partially deformed by the annealing process (Figure 2.1d). Thus, 3D-printed ABS structures were pre-annealed at 130 ˚C in this study to avoid any overall structure deformations while also reducing surface complexity.

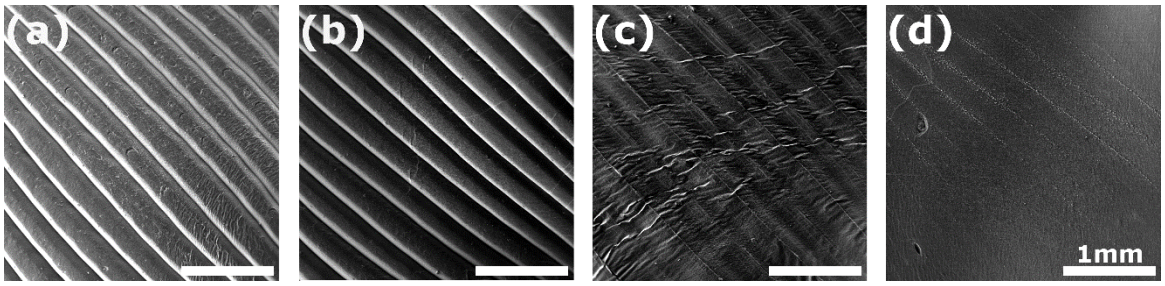


**Figure 2.1** SEM images of annealing pre-treated ABS polymer with (a) control, (b) 100 ˚C annealing, (c) 130 ˚C annealing and (d) 150 ˚C annealing samples. Pre-treatment annealing duration of 10 min.

Initial depositions were performed to optimize the alumina thin film coating on the ABS surface by examining cross sections created by mechanically snapping 3D-printed parts. When deposition temperatures above the $T_g$ were used with no pre-treatment annealing, sub-surface aluminum centres were found and thinner layers were formed (Figure 2.2a), suggesting infiltration of the precursors into the bulk of the substrate. However, the various pre-annealed samples (Figure 2.2b-d) showed increased aluminum content on the surface with little to no sub-surface aluminum centers, showing that pre-annealing could prevent substantial infiltration. Hence, 130 ˚C pre-treatment annealing preformed in this study provided favourable alumina coating conditions and limited infiltration into the bulk material.

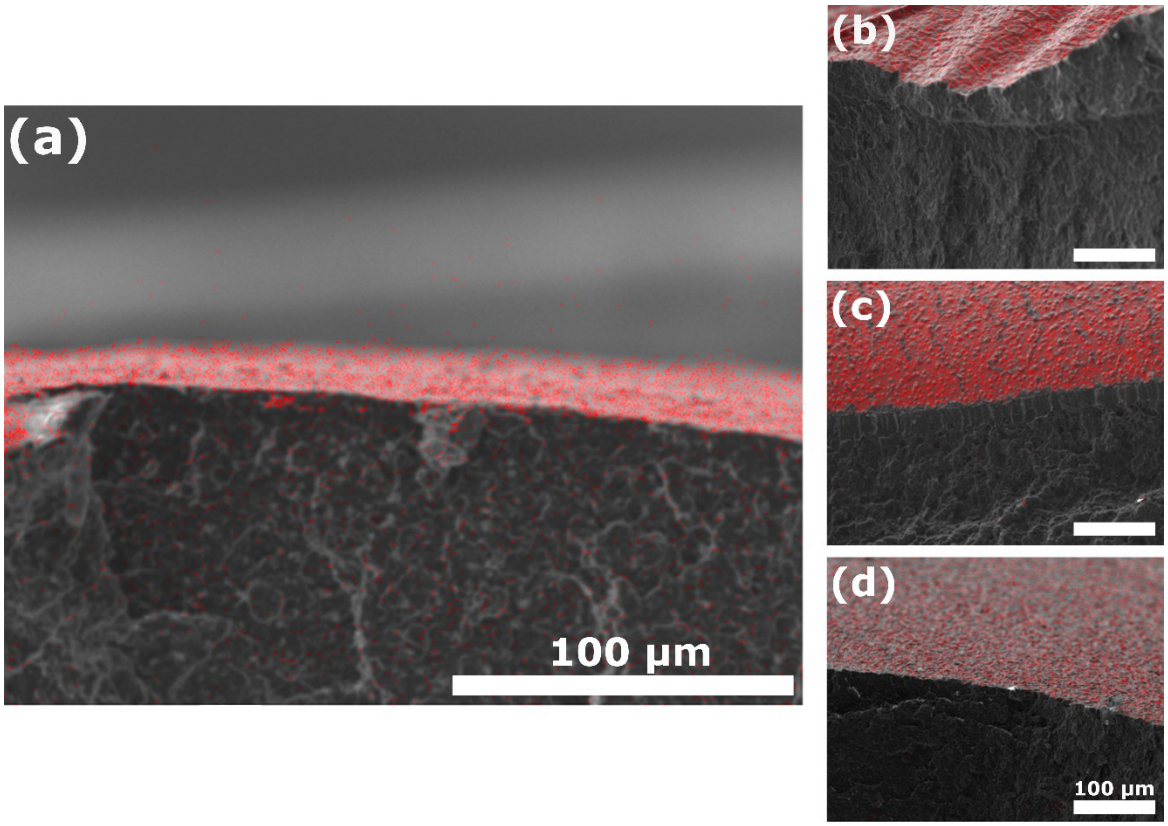


**Figure 2.2** EDS mappings of aluminum content overlayed on SEM images of annealing pre-treated ABS polymer cross sections after deposition using ABS-1 pulse program. With (a) control, (b) 100 ˚C annealing, (c) 130 ˚C annealing and (d) 150 ˚C annealing coated samples. Red dots indicated aluminum concentration.

Below the glass transition temperature, the polymer structure is more rigid and has smaller polymer chain spacings[62] which (combined with the pre-treatment annealing) in turn creates a less porous surface for the precursors to react with.[63] This highlights two aspects of thin film deposition observed on an ABS polymer substrate: deposition above the glass transition temperature can allow infiltration, and pre-annealing above this temperature can mitigate it. This gives us control over the deposition going forward and will also allow us to study infiltration (in a future project).

Thus, an optimal deposition temperature was found to be 80 °C (ABS-5). This deposition temperature is 25 ˚C below the $T_g$ of ABS, which aided in the preferential coating of the polymer surface rather than allowing any infiltration of the precursors into the substrate bulk, while giving a well-controlled conformal ALD coating.

Using a standard deposition of 1500 cycles, with 0.1 s pulses of TMA and water, separated by purges of 20 s (after TMA) and 40 s (after water), a growth per cycle of 1.35 Å was found. Notably, the white color of the ABS structures very slightly yellowed after deposition. An adhesion tape test was performed to better understand how well the alumina thin film adhered to the polymer ABS surface.[9] A piece of 3M Conductive Adhesive Transfer Tape (the same tape which is used to adhere a sample to the SEM stage platform) was firmly pressed onto ABS-5 and removed shortly after with a pair of forceps. The resultant area underneath showed no macroscopic signs of physical or color change.

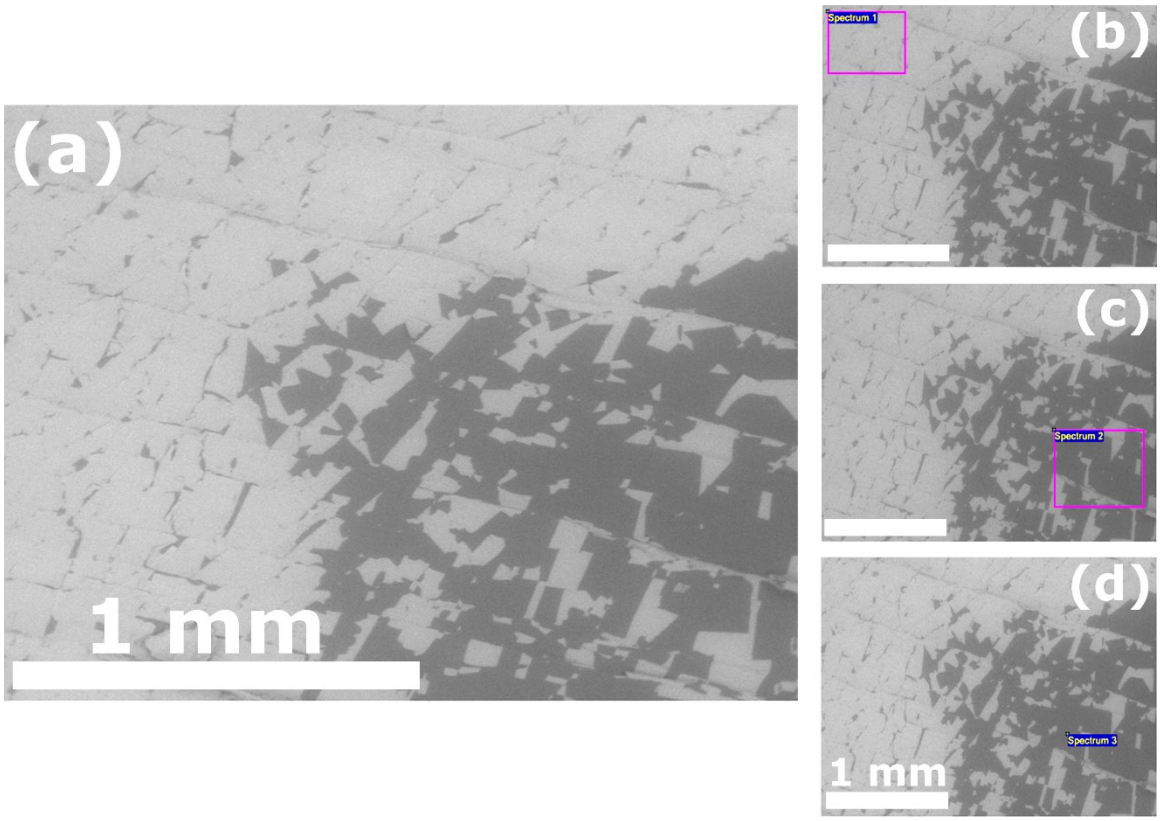


**Figure 2.3** SEM backscatter image of a coated ABS surface using ABS-5 recipe, with bottom right quadrant been where the tape was applied and then subsequently removed (a). Selective EDS scanned regions on tape test sample with (b) unaffected Spectrum 1 area, (c) affected Spectrum 2 area and (d) Spectrum 3-point scan in effected area.

Upon examination of this sample via SEM, the tape appeared to have removed a significant portion of the alumina film on the surface (Figure 2.3a). The darker regions show regions where the film was lifted by the tape. EDS analysis was used to differentiate these regions to further investigate the surface composition (Figure 2.3b-d). Three spectrum scans were performed, where the third scan was a point scan directly in the middle of a large dark region, to limit the software's "collection window". The data collected by the point scan likely represents a truer elemental composition of the areas where $Al_2O_3$ exfoliation was seen.

**Table 2.3** EDS tabulated data from Figure 2.3. Spectrum scans on coated ABS tape test sample.

| Element | Unaffected (Figure 2.3b) | | Adhesion (Figure 2.3c) | | Point Scan (Figure 2.3d) | |
|---|---|---|---|---|---|---|
| | Weight % | Atomic % | Weight % | Atomic % | Weight % | Atomic % |
| Aluminum | 37.0 | 24.2 | 16.3 | 8.9 | 14.1 | 7.5 |
| Carbon | 17.0 | 25.0 | 48.6 | 59.1 | 53.4 | 63.5 |
| Oxygen | 46.0 | 50.8 | 35.1 | 32.0 | 32.5 | 29.0 |

Looking at the aluminum content (Table 2.3), the exfoliated region (Figure 2.3c) had just over half of the aluminum content compared to the intact region (Figure 2.3b). However, as indicated from the point scan (Figure 2.3d) there was still a measurable concentration of aluminum on the surface even in the exfoliated regions. This is corroborated by the loss of oxygen in the exfoliated region and in the point scan. The increase in carbon content in the exfoliated region is complicated by the nature of the data collection. Since the EDS measures deeply into the film and substrate (estimated to be on the order of 0.3 – 2 μm at 5 – 20 keV), the increase in carbon could be due to loss of aluminum and oxygen in the film, with the software automatically balancing the measured elements to 100 %. Conversely, it might be caused by residual adhesive left behind by the tape test. This becomes clearer examining the oxygen content: if the exfoliated region indicated the removal of alumina from the surface, the loss of oxygen should be proportionate to the loss of aluminum (i.e., 2:3 Al:O, since there is no oxygen in the ABS polymer).[61] However, there is a larger oxygen concentration in the adhesion region that is not consistent with the $Al_2O_3$ ratio. This ultimately suggests that increases seen in carbon and oxygen are – at least in part – due to residual adhesive.

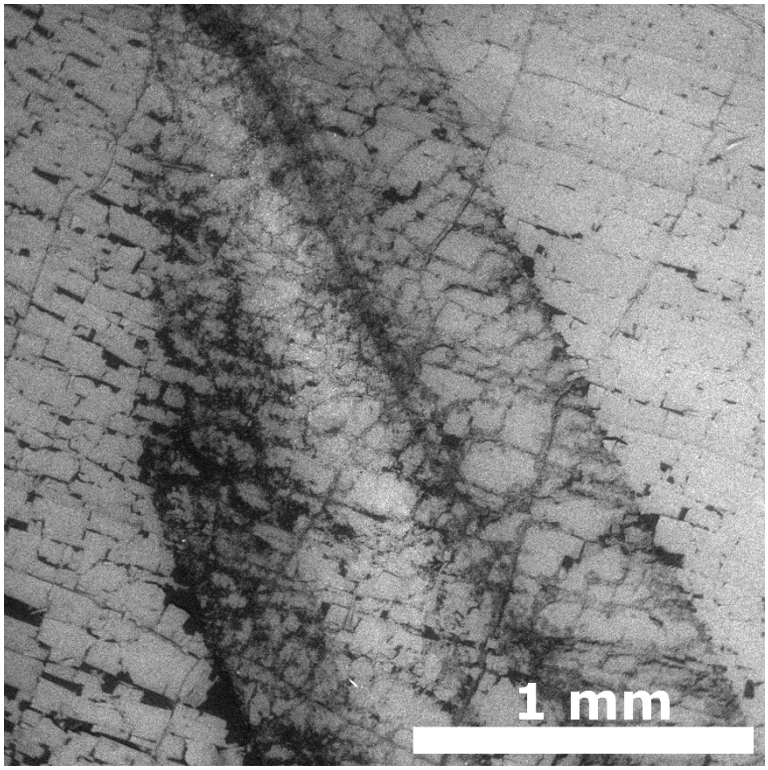


**Figure 2.4** SEM backscatter image of coated ABS surface using ABS-5 pulse program with scratched surface using forceps.

A scratch test was also performed to investigate both adhesion and composition, by creating a 1 cm long gouge with forceps in the surface of the polymer structure. There was no observable macroscopic physical change to the surface of the structure after the test and the material remained the same color. As seen from the SEM image, the gouge (darker region running diagonally across the center of the image in Figure 2.4) is about 1.5 mm in diameter. The soft texture of the ABS allowed the forceps to create a trench during the scratch. At first glace it also appears the $Al_2O_3$ coating is still present on the surface and just deformed in accordance with the morphed surface rather than being removed.

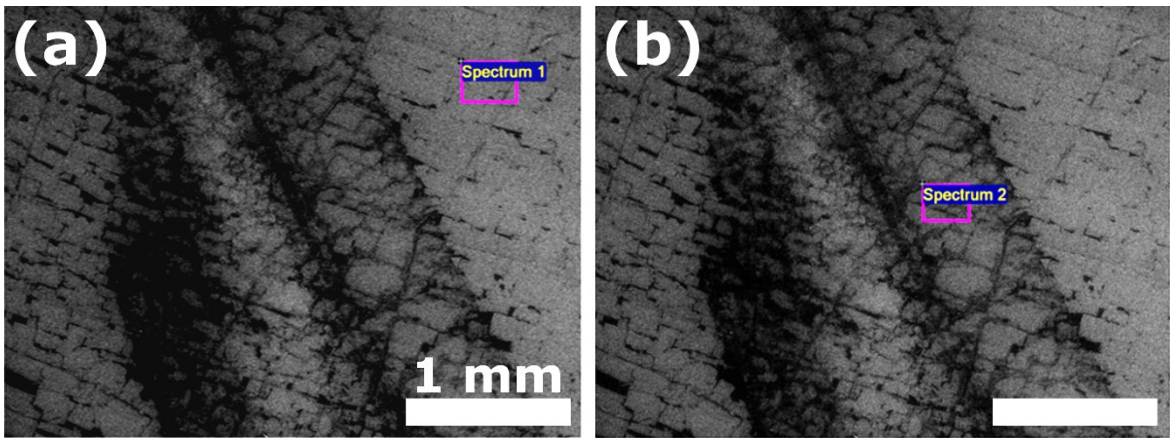


**Figure 2.5** SEM backscatter images of selective EDS scanned regions on ABS coated scratch test sample with (a) unaffected Spectrum 1 area, (b) affected Spectrum 2 area.

Two EDS spectra were taken outside and inside the affected scratch area (Figure 2.5a and Figure 2.5b respectively), to compare and contrast the two regions. Tabulated data for each region is shown in Table 2.4 below.

**Table 2.4** EDS tabulated data from Figure 2.5. Spectrum scans on coated ABS scratch test sample.

| Element | Unaffected Area (Figure 2.5a) | | Gouge (Figure 2.5b) | |
|---|---|---|---|---|
| | Weight % | Atomic % | Weight % | Atomic % |
| Aluminum | 38.0 | 25.1 | 35.2 | 22.6 |
| Carbon | 15.4 | 22.9 | 19.8 | 28.6 |
| Oxygen | 46.6 | 52.0 | 45.0 | 48.8 |

The $Al_2O_3$ coating was well adhered to the ABS surface (Table 2.4). The scratch test showed far less loss of alumina when compared to the tape test, with only a minor loss of Al (2.5%) and O (3.2%), with the ratio in loss (2:2.6 Al:O) suggesting $Al_2O_3$ was scratched off. The increase in carbon content here can is ascribed to the relative decrease of the $Al_2O_3$ signals and thus increase in carbon: since the percent composition is inherently set to 100%,

any loss of Al and O will be reflected by an increase in C. However, the small drop in aluminum and oxygen content and increase carbon content shows that the surface was much more resistant to scratching than to the peeling of the strong binding conductive transfer tape (adheres to surfaces much stronger than Scotch tape) used in the tape test. None the less, both the tape and scratch tests demonstrate that the alumina remains adhered to the underlying ABS substrate.

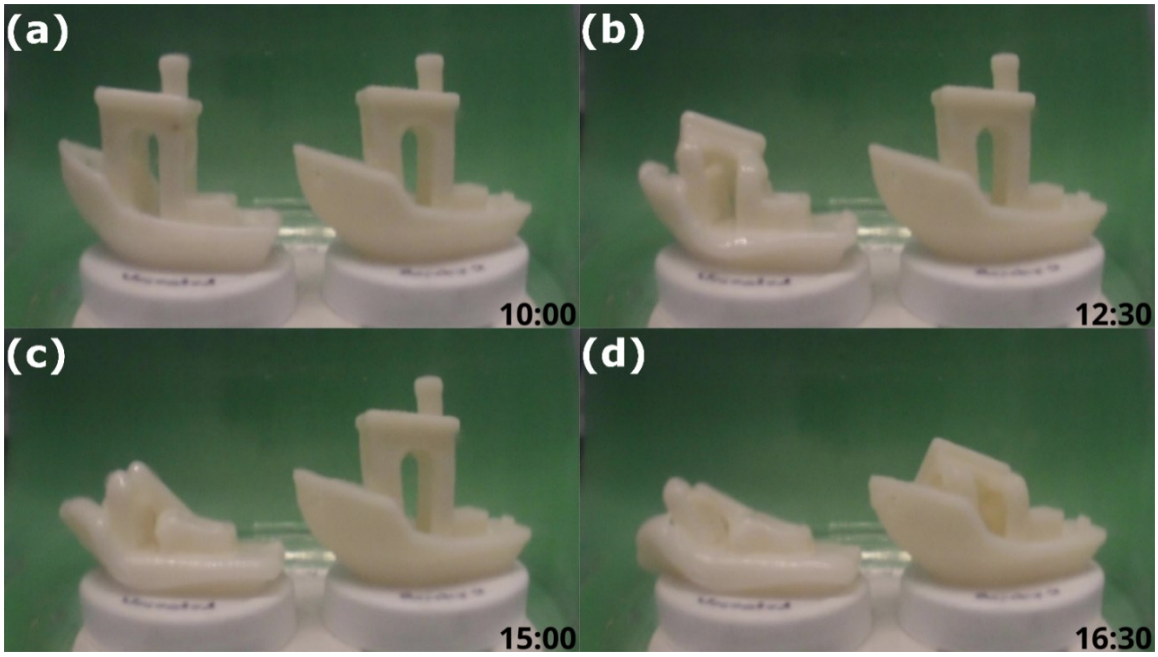


**Figure 2.6** Frame grabs from ABS Benchy exposure to acetone during solvent resistance experiment where the left Benchy is uncoated, and the right is coated using ABS-B1 process. Timer in bottom right of each image represents time elapsed in hours since experiment start. (a) first sign of uncoated structure deformation after 10 hr. (b) uncoated structure collapse after 12.5 hr. (c) first sign of coated structure deformation after 15 hr. (d) coated structure collapse after 16.5 hr.

Given the robustness of the alumina coating, an experiment was performed to examine its protective ability with respect to solvent infiltration. ABS can be easily structurally weakened by swelling caused by solvent uptake from vaporous solvents like acetone. This is commonly preformed after 3D printing ABS structures, exposing the structure to small amounts of acetone vapours for a short period of time will smoothen the extrusion lines

and create a smooth surface. A 3D-printed "Benchy" structure[64] was chosen, since it is a commonly used benchmark in 3D printing testing and optimization due to its quick printing time and number of delicate features like thin supports and overhangs. Two structures were printed in ABS, an untreated one (B1), and one annealed as a pre-treatment and then coated using the same pulse program as used in ABS-B5 (B2). Both structures were placed on a stage in a desiccator with ~20 mL of acetone at the bottom. A timelapse of solvent exposure was recorded (Figure S6.1 of Varga C. A. and Barry S. T.[65]). The uncoated B1 (left most, Figure 2.6) was deformed and affected by the acetone vapors much sooner than B2 (right most, Figure 2.6). Individual frames from the timelapse were isolate to show the times at which the structures showed signs of initial deformation (Figure 2.6a and Figure 2.6c), with the untreated B1 deforming after 10 hours and the pretreated and coated B2 deforming after 15 hours. Complete structure collapse (Figure 2.6b and Figure 2.6d) was seen for B1 at 12.5 hours and at 16.5 hours for B2. This effectively demonstrates that under high acetone vapor concentrations, the coated B2 had significantly better solvent resistance and outperformed the uncoated B1 by around 150%. A separate control solvent exposure experiment was also conducted by pre-treating a third structure (B3) in the same conditions as B2, but without an alumina coating. Structure B3 was further annealed at 130 ˚C and placed in an oven at 80 ˚C for 24 hr (to emulate the reaction chamber conditions during $Al_2O_3$ deposition). This annealing and further thermal treatment had no significant effect on B3 with respect to the solvent exposure experiment: deformation was still seen after 10 hours with structural collapse occurring after 12.5 hours, like was seen for B1. This initial solvent exposure experiment demonstrates the promise of ALD post-processing for additive manufacturing. Further research into the effects of infiltration, as well as control over thermal properties (like the glass transition temperature) are ongoing.

## 2.4 Summary and Conclusions

A coating deposited via atomic layer deposition on a 3D-printed ABS polymer structures provided a well-adhered protective layer against initial acetone solvent exposure. The coated ABS polymer structures were able to withstand the high acetone vapours for a period of 15 hours, 5 hours longer than compared to an uncoated sample. This proof of concept demonstrates how 3D printing combined with ALD overcoating can create a robust

and resistant protective coating on polymer architectures while still maintaining to a low cost and easily accessible manufacturing process. Which could provide an alternative to metal architectures where polymers could not be used due to damaging conditions such as solvent vapours show in this work.

# Chapter 3

# Reversable Alteration of 3D Printed Polymer Properties via Infiltration of Alumina by Atomic Layer Deposition

*Reprinted from the original manuscript:*

Atilla C. Varga[a] and Seán T Barry.[a] Reversable Alteration of 3D Printed Polymer Properties via Infiltration of Alumina by Atomic Layer Deposition. *Submitted*.

[a] Department of Chemistry, Carleton University, 1125 Colonel By Drive, Ottawa, Ontario, K1S 5B6, Canada

## 3.1 Introduction

3D Printing or additive manufacturing has become popular in recent years in not only the hobbyist and industrial fields as a rapid cost-effective manufacturing process, but also in scientific research.[31,32] The ability to rapidly model and print 3D objects allow for an iterative design process ideal for developing new technologies and processes which range from pharmaceuticals[66], energy storage[37,39,67] and catalysis.[36] Hence the easy-to-use 3D printer has become common in many scientific laboratories[40] not to mention the many uses of easily accessible printable laboratory equipment and parts.[35]

Atomic layer deposition (ALD) is a layer-by-layer thin film deposition process for growing conformal, uniform, and controllable inorganic thin films.[59] As a result, ALD can not only be used on dense rigid substrates but also on high aspect ratio and porous surfaces.[68,69] This makes it ideal for use with polymers which can have large polymer strand spacings, hence a mesoporous nature. This porosity allows for the ALD precursors to diffuse into the polymer substrate during deposition; a process known as infiltration.[70] The product of organic-inorganic hybrid polymer materials created using ALD infiltration are interesting and exciting due to their unique structure and properties.[15,30,71] Such interesting materials have applications in solar cells[72], vapour/gas diffusion barrier[14], energy storage, and catalysis.[73]

Many factors play a role in the infiltration of ALD deposited material into a 3D printed polymer substrate: both temperature and inhibition from a surface coating have been previously investigated by our group.[65] For consistency with our previous work, the polymer substrates used in this work will undergo ALD deposition by $Al_2O_3$ using trimethylaluminum(III) (TMA) and water. This prototypical ALD target film using well-defined precursors lends itself to straightforward film characterization and control over the deposition process, since alumina deposited by this process has been thoroughly investigated on a variety of substrates, including polymers.[61] The deposition can be performed thermally with a wide range of deposition temperatures making it amenable to various 3D printing polymers. The thermal process also eliminates the need and concern

of using a plasma treatment which could be damaging the 3D printed structures during the deposition process.

The glass transition temperature ($T_g$) of a polymer is the temperature at which the amorphous polymer transitions from a rigid, brittle (or glassy) state to a soft, rubbery (or viscous) state.[74,75] The $T_g$ of a polymer can be and is most commonly determined via the use of differential scanning calorimetry (DSC).[76] In the DSC trace, a glass transition is indicated by a baseline shift or step change (as seen in Figure 3.1) in which the $T_g$ is the inflection point (or mid point) within the step change.[53,54] Therefore each polymer has a unique and reversable $T_g$ which will be measured using DSC to observe the infiltration effects of $Al_2O_3$ into 3D printed polymers.

Acrylonitrile butadiene styrene (ABS) and polyvinyl alcohol (PVA) will be used as the selected 3D printing polymers (filament) due to their commonality and for consistency with our previous work, to provide a general framework and understanding of how ALD effects and behaves with 3D printed polymers. Pure ABS has $T_g$ of ~105 ˚C[60] which matches the filaments $T_g$ at ~104 ˚C.[77] For PVA the $T_g$ can vary, where pure PVA is at ~81 ˚C[78] and the filament ranges from 45-68 ˚C.[38] This discrepancy is likely due to impurities found within the filament which are introduce during production (such as polyvinyl acetate, vinyl esters or ethyl acetate)[38] since the purity of filaments is not very high as it is not crucial for 3D printing use. It is important for this work to use commercially available filaments (and accept these impurities) to better inform the practical application of ALD to additive manufacturing.

## 3.2 Experimental

Unless otherwise noted, all reagents were purchased from commercially available sources and used as received (Sigma Aldrich and Strem Chemicals). 3D-printed structures were supplied by Kromati.ca using a white ABS polymer (Prusament ABS) or a clear PVA polymer (PrimaSelect PVA+). ABS structures were printed in an enclosure using 100 ˚C heated bed temperature and 255 ˚C nozzle temperature. PVA structures were printed in an open enclosure using 60 ˚C heated bed temperature and 210 ˚C nozzle temperature. PVA

filament was stored between printing in a sealed vacuum bag to prevent the hydroscopic polymer from absorbing additional moisture.

ALD experiments were carried out using a Picosun R-200 Standard ALD tool. Depositions were carried out using Trimethylaluminum (97 %, Aldrich), $H_2O$ (HPLC grade, Aldrich), and a carrier gas of dinitrogen (>99.9999 %, Praxair). Process parameters included an intermediate space flow of 600 SCCM, stabilization time of 60 min, and flow rate of 150 SCCM and 200 SCCM for TMA and $H_2O$ respectively.

Deposition process parameters for each polymer were as follows:

**Table 3.1** List of ALD infiltration recipes with process parameters used for ABS and PVA polymer structures. *X* and *Y* variables in run name correspond to number of cycles, which varied from 5-500 for both ABS and PVA.

| Run | TMA | | $H_2O$ | | Temperature / ˚C | Soak Time / s | Cycles |
|---|---|---|---|---|---|---|---|
| | Pulse / s | Purge / s | Purge / s | Purge / s | | | |
| ABS-*X* | 0.1 | 20.0 | 0.1 | 40.0 | 130.0 | 60.0 | *X* |
| PVA-*Y* | 0.1 | 40.0 | 0.1 | 90.0 | 80.0 | 60.0 | *Y* |

For each polymer (ABS and PVA) two printed yet uncoated samples were used to determine the $T_g$ of the polymer pre-deposition. Samples were small puck-shaped cylinders with a 5 mm diameter and were 2.5 mm high. One set was used as is after printing (named **ABS-U** and **PVA-U**) and the other set was placed in an oven at the ALD deposition temperatures for the same duration of time as the depositions, to account for these temperature effects (named **ABS-U-PH** and **PVA-U-PH**). This ensures that all samples underwent the same printing process and one reference set experienced deposition conditions to confirm the change in $T_g$ observed is compared to a true reference. Hence any change in $T_g$ will be from the alumina infiltration and not printing or deposition conditions.

Sample preparation for SEM and EDS analysis involved mechanically breaking the 3D printed structures to reveal the cross section followed by coating the ABS or PVA samples with a layer of carbon film for better conduction. This was done using a Quorum Q150T ES sputter/evaporator tool by evaporating a carbon layer using graphite. SEM imaging was performed using a Tescan Vega-II XMU VPSSEM tool in both secondary electron and backscatter electron imaging modes with a working distance of ~ 10 nm and accelerating voltage of 10 kV for all scans. EDS data collection was performed in conjunction with SEM imaging using an Oxford Instruments Inca EDS tool.

DSC experiments were performed on a TA Instruments Q100 apparatus with a refrigerated cooling system (RCS) accessory and using Q Series pressure cells as the compound holder and reference. A purge gas of dinitrogen (>99.999 %, Praxair) was used at a flow rate of 50 mL/min. Ramp experiments were performed with a ramp rate of 10 ˚C/min. The data which was recorded during the experiments was also analyzed using TA Universal Analysis software, which was also used to calculate the polymer materials $T_g$.

## 3.3 Results and Discussion

The selected polymers (ABS and PVA) were first examined by DSC to investigate the $T_g$ of the as-printed polymers compared to that of the pre-printed and pure polymer literature values. The as-printed DSC is shown by the green traces in Figure 3.1 for both ABS and PVA with the calculated $T_g$ values and averages shown in Table S6.1 and Table S6.2 respectively. Other polymers were also examined (PLA and TPU) which resulted in very little to no infiltration observed and were hence not included in the data.

The $T_g$ for ABS-U is slightly lower (103.43 ± 0.43 ˚C) than the expected literature value of pure ABS at ~105 ˚C[60], but it is within an acceptable range of the ABS filament (~104 ˚C).[77] The probable reason for the difference between the $T_g$ of the filament and pure polymers is the presence of additives.[79] These additives are used to alter the filaments color, reduce the emission of volatile organic compounds (VOCs), improve the materials strength and durability, and to optimize the filaments printability (promote better layer adhesion, reduce warping, etc.). Since the exact composition of the filament is not known or provided

by the manufacturer, the specific additive(s) which are responsible for the difference were not identified.

For PVA the difference in $T_g$ between the pure polymer and filament can vary drastically with the $T_g$ of pure PVA reported as ~ 81 ˚C[78] and the filament ranging from 45-68 ˚C.[38] As mentioned previously the reason for the range in $T_g$ for PVA is the hydroscopic nature of the polymer, where the higher the moisture content in the polymer the lower the $T_g$. The rate at which water is absorbed by PVA depends on the composition of the material. Where pure PVA can uptake water at a rapid rate resulting in a maximum moisture content of 42% just after 4 hr following a logarithmic trend; compared to 3D printing PVA filaments, which have additives to limit and slow its hydroscopic nature result in a much slower water uptake.[78] Unfortunately the rate at which water uptake occurs is not known for the specific filament used in this thesis. Hence the $T_g$ of the PVA filament was compared to the literature values range to qualitatively determine the moisture content. The DSC trace of the as-printed polymer is shown in Figure 3.1b and the calculated and averaged value of PVA-U was determined to be (48.34 ± 0.45) ˚C. When compared to literature values, 48 ˚C is on the lower end of the filament's literature $T_g$ range (45-68 ˚C[38]) which corresponds to a high moisture content most likely due to the storage and handling of the filament and printed structures. The filaments were stored in a vacuum sealed bag, however there was no heating or baking of the filament prior to printing. Meaning, each time the filament was used or taken out of the bag it slowly absorbed moisture over time which could have accumulated and was not removed (dried out). This becomes more evident when looking at the pre-heated samples.

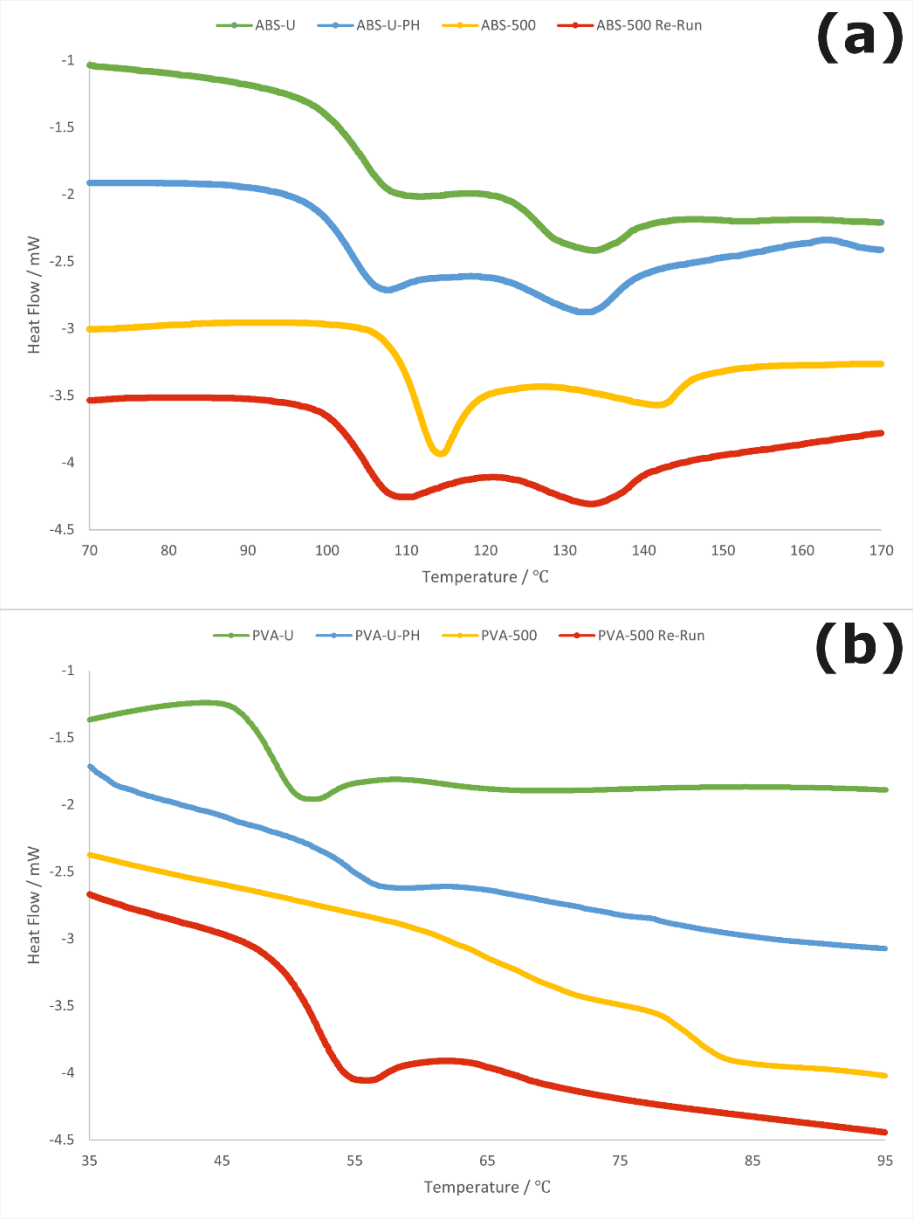


**Figure 3.1** DSC traces in order from top to bottom of uncoated (U), uncoated plus pre-heated (U-PH), after 500 ALD cycles (500) and recollected 500 ALD cycles after one DSC ramp cycle (500 Re-Run) polymer samples. Where (a) is the ABS polymer samples and (b) is the PVA polymer samples.

For each of the polymers the pre-heating process had differing outcomes on the DSC trace and $T_g$ which can be seen in Figure 3.1 by comparing the green uncoated sample) trace to the blue trace (uncoated pre-heated sample). For **ABS-U-PH** the pre-heating process had

no significant effect on the $T_g$ of the polymer which is clearly visible when comparing the two DSC trances in Figure 3.1a. The step change begins just after 90 ˚C for both samples and have inflection points around 104 ˚C. Comparing the calculated and averaged $T_g$ values reveals the same consistency with the $T_g$ for **ABS-U** being (103.43 ± 0.43) ˚C and **ABS-U-PH** (103.15 ± 0.14) ˚C. As for PVA, the pre-heating had a significant effect on the samples again due to the hydroscopic nature of the polymer.[80] From Figure 3.1b, the two DSC traces have noticeable step changes which are just under 10 ˚C apart. Comparing the calculated $T_g$ values there was a difference of ~ 6.5 ˚C between the $T_g$ of **PVA-U** and **PVA-U-PH**. During the pre-heating process, any moisture which was absorbed would have evaporated.[81] The duration of this pre-heating process also affects the moisture content within the polymer. Although **PVA-U** underwent heating to 210 ˚C during printing, the filament was only heated in the printer's nozzle for a few seconds; not enough time to dry the polymer completely. Compared to duration of the pre-heating process where deposition conditions are mimicked (with temperatures held constant throughout the reactor space flushing, equilibration and deposition time which accumulates to 4 hours), this difference in time accounts for the higher $T_g$.

Knowing the appropriate uncoated $T_g$ values for each polymer, a series of depositions were undertaken to investigate how the number of ALD cycles effects the $T_g$ of the 3D printed polymers. The number of ALD cycles ranged from 5-500 with varying results for each polymer. For each variance in cycle number, a series of ABS and PVA samples were examined by DSC to determine the $T_g$ which were averaged and plotted against cycle number and are shown in Figure 3.2 and Figure 3.3 respectively.

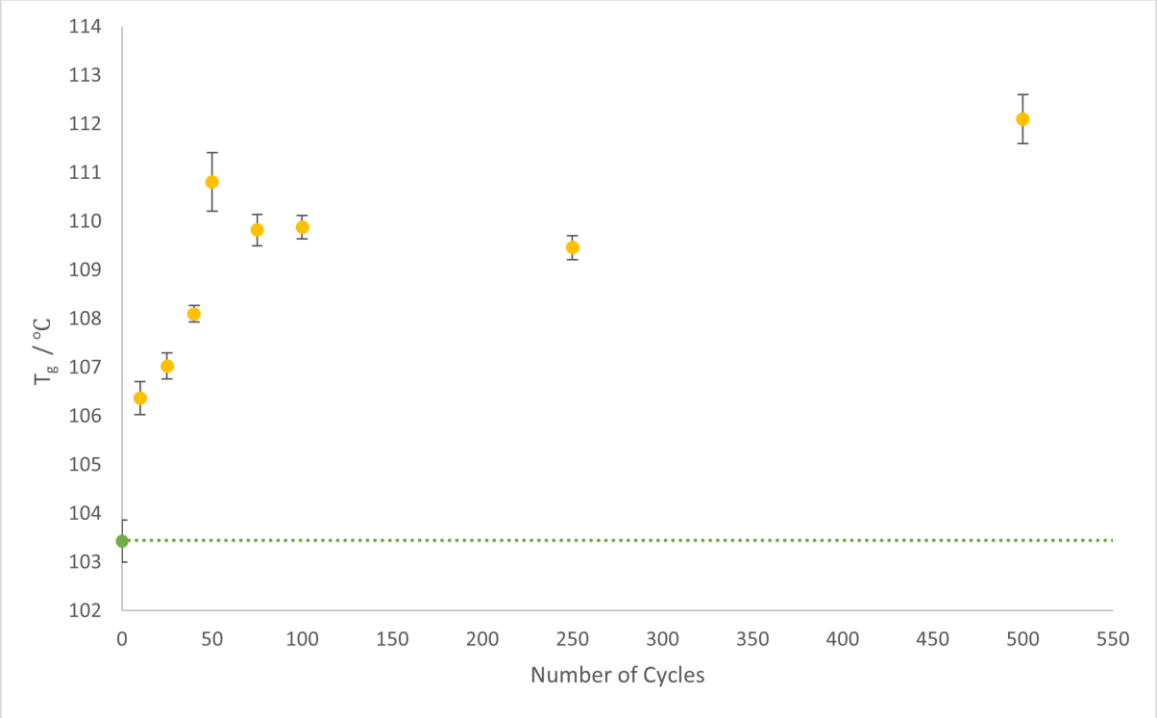


**Figure 3.2** DSC calculated and averaged $T_g$ of ABS polymer samples with errors bars showing standard deviation. Yellow points indicated coated ABS samples and the green dotted line indicates the $T_g$ value of ABS-U. The x axis represents the number of ALD cycles the individual polymer samples underwent.

Initial low cycle-number depositions on ABS showed a change of 4 ˚C in the $T_g$ with a corresponding increasing trend vs cycle number which can be seen in Figure 3.2. As the number of ALD cycles increased, the increasing trend begins to plateau indicating the positive impact of continued deposition on the $T_g$ of ABS diminishes at high cycle numbers. This could be caused by the polymer surface being eventually covered in a limiting thin film layer preventing the further infiltration of precursor after about 50 cycles. The chemical structure of ABS is not ideal for alumina infiltration and nucleation due to the lack of carbonyl and hydroxy functional groups to act as nucleation sites. Hence additional growth in subsequent cycles favours creating alumina particles within the polymer substrate or on the surface coating where additional precursor can better bind to free hydroxy functional groups (this is corroborated by EDS mapping, *vide infra*). Although the system has a high exposure of precursor with long soak times, the rate at

which alumina grows on the polymer is much lower than it grows on an alumina surface.[10,11] This is the reason for better surface film growth which then inhibits precursor diffusion into the polymer. Therefore, the $T_g$ of ABS after 500 cycles was (112.10 ± 0.50) ˚C which is just under a 9 ˚C difference compared to the uncoated sample, within error.

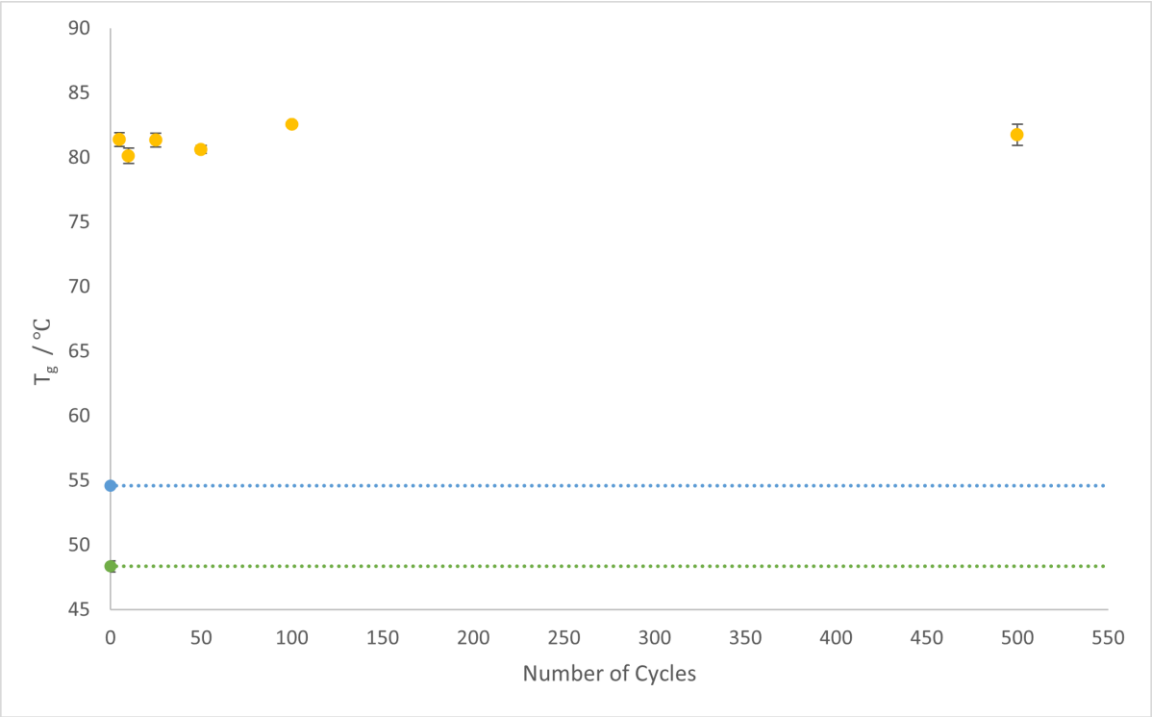


**Figure 3.3** DSC calculated and averaged $T_g$ of PVA polymer samples with errors bars showing standard deviation. Yellow points indicated coated PVA samples with green and blue dotted lines indicating the Tg of PVA-U and PVA-U-PH samples respectively. The x axis represents the number of ALD cycles the individual polymer samples underwent.

For PVA, the effect deposition had on the $T_g$ of the polymer was much more drastic and immediate compared to ABS, as seen in Figure 3.3. After just 5 cycles the $T_g$ increased from (54.60 ± 0.09) ˚C to (81.38 ± 0.55) ˚C, an increase of ~ 26 ˚C from **PVA-U-PH** to **PVA-5**. The effect further cycles had on the $T_g$ was not significant, shown clearly in Figure 3.3, with each data point being just above 80 ˚C, with very small error bars. Even after 500 cycles the $T_g$ of PVA remained at (81.74 ± 0.82) ˚C, indicating that in this case the limiting factor for further infiltration into the polymer substrate is the availability of polymer binding sites. This is the opposite case as from ABS since the chemical structure of PVA

has many hydroxy functional groups and allows for better alumina infiltration growth. Once the polymers hydroxy groups are saturated, the effect of further deposition has no significant change on the $T_g$. Even with a thicker surface coating and larger alumina clusters found in open voids within the polymer (seen by EDS mapping, *vide infra*), the $T_g$ is not significantly altered. Hence drawing further understanding that the alteration deposition has on the polymers $T_g$ is not from the amount of infiltration or film growth but rather the amount of growth directly on the polymer structure which causes the $T_g$ alteration. Otherwise, if the former were the case, we would expect the $T_g$ of the PVA samples with higher cycle numbers to have a significantly higher $T_g$ due to the larger alumina surface coating and particles.

The $T_g$ of a polymer by definition is a reversable transition point which when measured via DSC will give virtually the same value. This is not the case however with the ALD altered polymers in this work. As in once the modified polymers $T_g$ is surpassed, the $T_g$ for each polymer changes to a different value than firstly measured. After the initially DSC ramp where samples underwent heating past the newly altered $T_g$ (to 200 ˚C) and then cooled, the reversibility of the altered $T_g$ was lost. This can be seen for both ABS and PVA in Figure 3.1 where after one DSC ramp cycle, the $T_g$ of the polymer reverts back to with a few degrees of the original uncoated pre-heated polymer. For **ABS-500 Re-Run** the $T_g$ and DSC trace matches very well with **ABS-U-PH** and along with **ABS-U**. The same can be seen for PVA by comparing **PVA-500 Re-Run** to **PVA-U-PH** where the $T_g$ and DSC trace align very well and only differ by a few degrees. Thus, indicating that the original effect of deposition on the polymers $T_g$ is lost after just one heat cycle for both ABS and PVA. In addition, the number of cycles each polymer sample underwent did not have any effect on the value of the reverted $T_g$ (hence the highest cycle number is shown in Figure 3.1) and all the re-run samples came within 2-3 ˚C of the pre-heated pure polymers $T_g$. The mechanism for why this occurs is not fully understood and will be investigated further however one possible explanation is that much like during an annealing process, the infiltrated Alumina percolates to the surface or creates larger nanoparticles within the polymer which then have less of an effect on the $T_g$ in successive heat cycles.

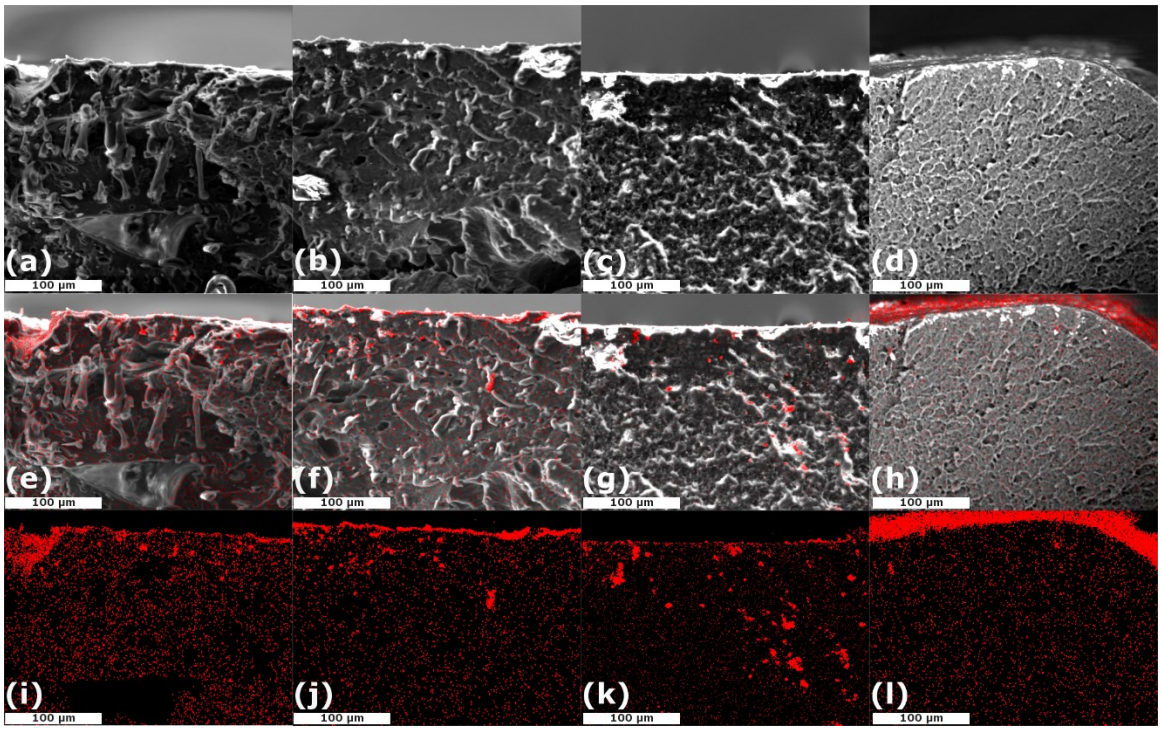


**Figure 3.4** Cross sectional SEM images, EDS aluminum mappings and mix images for lowest and highest ALD cycle number for PVA and ABS. Where first column is for PVA-5 sample, second column is PVA-500, third column is ABS-10 sample and fourth column is ABS-500 sample. First row shows 1000x magnification SEM images, second row shows SEM and EDS mapping mix images, and third row shows EDS mappings where red dots indicate aluminum concentration.

After the polymers undergo varying numbers of deposition cycles, no noticeable changes to the polymer substrate are obvious from the cross sections. This can be seen by comparing Figure 3.4a to Figure 3.4b for PVA and Figure 3.4c to Figure 3.4d for ABS. Considering the EDS mappings of aluminum content, the difference between low cycle count and higher cycle count are significantly different for each polymer. For **ABS-10** (Figure 3.4g for mix and Figure 3.4k for mapping), there is a small coating layer on the surface with a significant amount of infiltration into the substrate. However, the infiltration into the polymer noticeably resulted in large particles or aggregation of alumina seen by the groupings of red dots. In comparison, **ABS-500** (shown by Figure 3.4h and Figure 3.4l) has a much

larger and thicker coating layer on the surface of the substrate. This change is not proportionate to the increased amount of infiltration in the substrate: the overall relative concentration is only slightly higher compared in **ABS-500** compared to **ABS-10**, whereas the clusters are larger. This is in accordance with the $T_g$ curves, where the plateau suggested that alumina grows better on itself, creating a thicker coating layer, which in turn limits the diffusion of precursor into the substrate. In addition, the particles within the polymer are larger compared to the overall infiltration concentration. Looking at the mappings for **PVA-5** (Figure 3.4i) it can be seen that a large, mostly uniform infiltration occurred, with some particle formation after just 5 cycles. There is also a very thin coating layer present indicated by the red horizontal line on the cross sections surface. Compared to **PVA-500** (Figure 3.4j) it can be seen that there is relatively the same amount of infiltration within the substrate. There is, however, a much more noticeable coating on the substrates surface in addition to an increased number and size of particles found within the substrate. Although more alumina is found on the surface and in clusters of this polymer, the Tg remained unchanged after the initial infiltration.

Comparing PVA to ABS, there is far better infiltration into the PVA substrate due to the more desirable hydroxy functional groups than in ABS, and so substantially better nucleation of alumina. The increased thickness of the surface coating is consistent with ABS and PVA since once a layer of alumina has grown on the polymer surface, infiltration drops off and there is no longer an effect on $T_g$.

## 3.4 Summary and Conclusions

Infiltration of alumina by ALD was successfully performed on 3D printed structures of ABS and PVA, and a change in $T_g$ was found for both polymer substrates. The $T_g$ of uncoated polymers were obtained using DSC before a series of depositions at varied cycle numbers were performed, ranging between 5-500 cycles. For ABS the correlation between cycle number and $T_g$ was positive before a plateauing, due to growth at the substrate surface and enhanced imbedded particle growth occurring, both of which inhibits additional precursor from infiltrating into the substrate and further affecting the $T_g$. For PVA, the infiltration occurred quicky and saturated most of the polymer after only 5 cycles where,

again further deposition did not alter the $T_g$. The reversibility of the new altered $T_g$ was lost as shown by DSC since each polymer reverted back to its original pre-heated $T_g$ after one heat cycle. Finally, the composition of the polymer structure is important for varying any physical properties such as $T_g$ while using infiltration by ALD, and polymer substrates providing good nucleation sites in the bulk of the polymer (like the carbonyl and hydroxyl moieties in PVA) should show a stronger response to the change in glass transition temperature due to enhanced infiltration.

# Conclusion and Further Directions

This thesis describes and outlines the integration of ALD on 3D printed models to create advanced and low-cost 3D printed architectures. Crucial experimental parameters to obtain preferential coating or infiltration of the target ALD material on the polymer substrate were discussed in general and discovered performing the deposition above or below the polymer substrates $T_g$. Process parameters such as soak time and pulse length were found to affect the amount of coating or infiltration observed in the polymer substrates, all of which can be applied to various other 3D printed polymer materials for various applications.

Coatings deposited via ALD on 3D printed ABS polymer structures provided a well-adhered protective overcoating layer which provided resistance against acetone solvent exposure. In a high acetone vapours environment, the coated ABS polymer structures were able to withstand periods of 15 hours, which was 5 hours longer than compared to an uncoated bare sample. The resultant overcoating was examined by EDS which yielded a 203 nm thin film with a 1.35 Å GPC. Both scratch and tape tests revealed that the overcoating was well adhered to the polymer surface. This protective overcoating could provide a cost effective and light weight alternative to metal architectures where polymers could not be used due to damaging conditions such as solvent vapours show by this work.

Infiltration of alumina by ALD were also successfully performed on ABS and PVA 3D printed structures, where a change in $T_g$ was found for both polymer substrates. Using DSC, the $T_g$ of uncoated and pre-heated polymers were obtained and compared to a series of depositions carried out at varied cycle numbers, ranging between 5-500 cycles. For ABS the infiltration had a positive ~ 9 ˚C effect on the $T_g$ at the highest cycle count when compared to the uncoated polymer. As for PVA, the $T_g$ of the infiltrated polymer increased ~ 27 ˚C when again compared to the bare polymer. The correlation between cycle number and $T_g$ was positive for both polymers before a plateauing at a certain level of infiltration. For ABS this plateau occurred due to preferential film deposition at the substrate surface, which inhibits additional precursor infiltration. For PVA, the infiltration occurred rapidly and saturated most of the polymer after only 5 cycles, after which additional deposition did

not alter the $T_g$. The gains in $T_g$ for both polymers were lost as shown by each reverting to their original $T_g$ values after one heat cycle when examined by DSC. The chemical composition of the polymer structures played an important role on varying the physical properties ($T_g$) since the more suitable functional groups found on PVA provided better binding sites for the TMA precursor than that of ABS. This gave the difference in a stronger response to the change in glass transition temperature due to enhanced infiltration seen in PVA compared to ABS.

Future work would include increasing the roadmap for ALD modified 3D printed architectures and exploring various applications. For the former, explaining why and how the $T_g$ reverts after one heat cycle would provide insight into the mechanism of precursor interaction and film growth on the polymer. This phenomenon may occur by the TMA initially reacting with the functional groups of the ABS structure (either the cyano, olefin or styrene) but in subsequent cycles preferentially reacting and growing a film on top of itself, since the binding environment is more favourable (due to the presence of hydroxyl functional groups and higher surface energy). This creates nucleation sites where larger clusters of alumina grow on the ABS structure. When the samples are heated, the nucleation can be cleaved, allowing mobility of the alumina clusters and thus reforming pure polymer. This creates a composite which does not affect the polymers Tg rather than a hybrid material.

An additional future direction is to expand to different polymer materials, providing a more concrete understanding and guidelines for how to use coating vs infiltration for thermal characteristic modification, as well as how each method is able to affect the polymers properties. This could be done by using polymers with different chemical structures and functional groups such as nylon, PC, etc. For the latter, taking the proof-of-concept solvent exposure experiment and modified $T_g$ could be applied to practical applications.

The most practical future direction for the lab would be to test the architectures in an ALD tool. The protective coating could be used for plasma resistance or the modified $T_g$ properties for use in higher temperature processes. The second direction could be for more industrial applications such as; use in space technology would be an ideal fit since the

polymer architectures could offer light weight alternative to metal and have a significant impact on cost.[82,83] Additional applications could focus on high surface area catalysis with nanoparticles grown on 3D printed polymers and conductive polymer networks used in batteries and/or solar cell applications for environmentally friendly and sustainable alternatives which can leverage 3D printing to be produced at scale with low cost.

# References


(1) Lee, J. Y.; An, J.; Chua, C. K. Fundamentals and Applications of 3D Printing for Novel Materials. *Applied Materials Today* **2017**, *7*, 120–133. https://doi.org/10.1016/J.APMT.2017.02.004.

(2) Wojtyła, S.; Klama, P.; Baran, T. Is 3D Printing Safe? Analysis of the Thermal Treatment of Thermoplastics: ABS, PLA, PET, and Nylon. **2017**, *14* (6), D80–D85. https://doi.org/10.1080/15459624.2017.1285489.

(3) Buchanan, C.; Gardner, L. Metal 3D Printing in Construction: A Review of Methods, Research, Applications, Opportunities and Challenges. *Engineering Structures* **2019**, *180*, 332–348. https://doi.org/10.1016/J.ENGSTRUCT.2018.11.045.

(4) Stansbury, J. W.; Idacavage, M. J. 3D Printing with Polymers: Challenges among Expanding Options and Opportunities. *Dental Materials* **2016**, *32* (1), 54–64. https://doi.org/10.1016/J.DENTAL.2015.09.018.

(5) Džunuzovič, E. S.; Džunuzovič, J. V.; Radoman, T. S.; Marinovič-Cincovič, M. T.; Nikolič, L. B.; Jeremič, K. B.; Nedeljkovič, J. M. Characterization of in Situ Prepared Nanocomposites of PS and TIO 2 Nanoparticles Surface Modified with Alkyl Gallates: Effect of Alkyl Chain Length. *Polymer Composites* **2013**, *34* (3), 399–407. https://doi.org/10.1002/PC.22423.

(6) Džunuzović, E.; Marinović-Cincović, M.; Vuković, J.; Jeremić, K.; Nedeljković, J. M. Thermal Properties of PMMA/TiO2 Nanocomposites Prepared by in-Situ Bulk Polymerization. *Polymer Composites* **2009**, *30* (6), 737–742. https://doi.org/10.1002/PC.20606.

(7) Radoman, T. S.; Džunuzović, J. V.; Jeremić, K. B.; Grgur, B. N.; Miličević, D. S.; Popović, I. G.; Džunuzović, E. S. Improvement of Epoxy Resin Properties by Incorporation of TiO2 Nanoparticles Surface Modified with Gallic Acid Esters.

*Materials & Design (1980-2015)* **2014**, *62*, 158–167. https://doi.org/10.1016/J.MATDES.2014.05.015.

(8) Sangermano, M.; Matucelli, G.; Amerio, E.; Bongiovanni, R.; Priola, A.; Di Gianni, A.; Voit, B.; Rizza, G. Preparation and Characterization of Nanostructured TiO2/Epoxy Polymeric Films. *Macromolecular Materials and Engineering* **2006**, *291* (5), 517–523. https://doi.org/10.1002/MAME.200500420.

(9) Kääriäinen, T. O.; Cameron, D. C.; Tanttari, M. Adhesion of Ti and TiC Coatings on PMMA Subject to Plasma Treatment: Effect of Intermediate Layers of Al2O3 and TiO2 Deposited by Atomic Layer Deposition. *Plasma Processes and Polymers* **2009**, *6* (10), 631–641. https://doi.org/10.1002/PPAP.200900038.

(10) Kemell, M.; Färm, E.; Ritala, M.; Leskelä, M. Surface Modification of Thermoplastics by Atomic Layer Deposition of Al 2 O 3 and TiO 2 Thin Films. **2008**. https://doi.org/10.1016/j.eurpolymj.2008.09.005.

(11) Wilson, C. A.; Grubbs, R. K.; George, S. M. Nucleation and Growth during Al 2O 3 Atomic Layer Deposition on Polymers. *Chemistry of Materials* **2005**, *17* (23), 5625–5634. https://doi.org/10.1021/CM050704D/ASSET/IMAGES/MEDIUM/CM050704DN00001.GIF.

(12) Lu, J.; Li, Y.; Song, W.; Losego, M. D.; Monikandan, R.; Jacob, K. I.; Xiao, R. Atomic Layer Deposition onto Thermoplastic Polymeric Nanofibrous Aerogel Templates for Tailored Surface Properties. *ACS Nano* **2020**, *14* (7), 7999–8011. https://doi.org/10.1021/ACSNANO.9B09497.

(13) Guo, H. C.; Ye, E.; Li, Z.; Han, M. Y.; Loh, X. J. Recent Progress of Atomic Layer Deposition on Polymeric Materials. *Materials Science and Engineering: C* **2017**, *70*, 1182–1191. https://doi.org/10.1016/J.MSEC.2016.01.093.

(14) Ferguson, J. D.; Weimer, A. W.; George, S. M. Atomic Layer Deposition of Al2O3 Films on Polyethylene Particles. *Chemistry of Materials* **2004**, *16* (26), 5602–5609.

https://doi.org/10.1021/CM040008Y/ASSET/IMAGES/LARGE/CM040008YF00009.JPEG.

(15) Gregorczyk, K.; Knez, M. Hybrid Nanomaterials through Molecular and Atomic Layer Deposition: Top down, Bottom up, and in-between Approaches to New Materials. *Progress in Materials Science* **2016**, *75*, 1–37. https://doi.org/10.1016/J.PMATSCI.2015.06.004.

(16) Parsons, G. N.; Atanasov, S. E.; Dandley, E. C.; Devine, C. K.; Gong, B.; Jur, J. S.; Lee, K.; Oldham, C. J.; Peng, Q.; Spagnola, J. C.; Williams, P. S. Mechanisms and Reactions during Atomic Layer Deposition on Polymers. *Coordination Chemistry Reviews* **2013**, *257* (23–24), 3323–3331. https://doi.org/10.1016/J.CCR.2013.07.001.

(17) Gordon, P. G.; Kurek, A.; Barry, S. T. Trends in Copper Precursor Development for CVD and ALD Applications. *ECS Journal of Solid State Science and Technology* **2015**, *4* (1), 3188–3197. https://doi.org/10.1149/2.0261501jss.

(18) George, S. M. Atomic Layer Deposition: An Overview. **1996**. https://doi.org/10.1021/cr900056b.

(19) Zhang, D.; Quayle, M. J.; Petersson, G.; Van Ommen, J. R.; Folestad, S. Atomic Scale Surface Engineering of Micro- to Nano-Sized Pharmaceutical Particles for Drug Delivery Applications. *Nanoscale* **2017**, *9* (32), 11410–11417. https://doi.org/10.1039/C7NR03261G.

(20) Oneill, B. J.; Jackson, D. H. K.; Lee, J.; Canlas, C.; Stair, P. C.; Marshall, C. L.; Elam, J. W.; Kuech, T. F.; Dumesic, J. A.; Huber, G. W. Catalyst Design with Atomic Layer Deposition. *ACS Catalysis* **2015**, *5* (3), 1804–1825. https://doi.org/10.1021/CS501862H/ASSET/IMAGES/LARGE/CS-2014-01862H_0013.JPEG.

(21) Peng, Q.; Sun, X. Y.; Spagnola, J. C.; Hyde, G. K.; Spontak, R. J.; Parsons, G. N. Atomic Layer Deposition on Electrospun Polymer Fibers as a Direct Route to Al2O3 Microtubes with Precise Wall Thickness Control. *Nano Letters* **2007**, *7* (3), 719–

722.
https://doi.org/10.1021/NL062948I/SUPPL_FILE/NL062948ISI20070118_035736.PDF.

(22) Puurunen, R. L. Surface Chemistry of Atomic Layer Deposition: A Case Study for the Trimethylaluminum/ Water Process. *J. Appl. Phys* **2005**, *97*, 121301. https://doi.org/10.1063/1.1940727.

(23) George, S. M.; Ott, A. W.; Klaus, J. W. *Surface Chemistry for Atomic Layer Growth*; 1996.

(24) Groner, M. D.; Elam, J. W.; Fabreguette, F. H.; George, S. M. *Electrical Characterization of Thin Al O Films Grown by Atomic Layer 2 3 Deposition on Silicon and Various Metal Substrates*; 2002; Vol. 413.

(25) Fabreguette, F. H.; Wind, R. A.; George, S. M. Ultrahigh X-Ray Reflectivity from Multilayers Fabricated Using Atomic Layer Deposition. *Appl. Phys. Lett* **2006**, *88*, 13116. https://doi.org/10.1063/1.2161117.

(26) Dendooven, J.; Detavernier, C. *Basics of Atomic Layer Deposition: Growth Characteristics and Conformality*; 2017.

(27) Hausmann, D. M.; Gordon, R. G. Surface Morphology and Crystallinity Control in the Atomic Layer Deposition (ALD) of Hafnium and Zirconium Oxide Thin Films. In *Journal of Crystal Growth*; 2003; Vol. 249, pp 251–261. https://doi.org/10.1016/S0022-0248(02)02133-4.

(28) Groner, M. D.; Fabreguette, F. H.; Elam, J. W.; George, S. M. Low-Temperature Al2O3 Atomic Layer Deposition. *Chemistry of Materials* **2004**, *16* (4), 639–645. https://doi.org/10.1021/CM0304546.

(29) Hemmen, J. L. van; Heil, S. B. S.; Klootwijk, J. H.; Roozeboom, F.; Hodson, C. J.; Sanden, M. C. M. van de; Kessels, W. M. M. Plasma and Thermal ALD of Al2O3 in a Commercial 200 Mm ALD Reactor. *Journal of The Electrochemical Society* **2007**, *154* (7), G165. https://doi.org/10.1149/1.2737629.

(30) Leng, C. Z.; Losego, M. D. Vapor Phase Infiltration (VPI) for Transforming Polymers into Organic–Inorganic Hybrid Materials: A Critical Review of Current Progress and Future Challenges. *Materials Horizons* **2017**, *4* (5), 747–771. https://doi.org/10.1039/C7MH00196G.

(31) Shahrubudin, N.; Lee, T. C.; Ramlan, R. An Overview on 3D Printing Technology: Technological, Materials, and Applications. *Procedia Manufacturing* **2019**, *35*, 1286–1296. https://doi.org/10.1016/J.PROMFG.2019.06.089.

(32) Lee, J. Y.; An, J.; Chua, C. K. Fundamentals and Applications of 3D Printing for Novel Materials. *Applied Materials Today* **2017**, *7*, 120–133. https://doi.org/10.1016/J.APMT.2017.02.004.

(33) Schubert, C.; Van Langeveld, M. C.; Donoso, L. A. Innovations in 3D Printing: A 3D Overview from Optics to Organs. *British Journal of Ophthalmology* **2014**, *98* (2), 159–161. https://doi.org/10.1136/BJOPHTHALMOL-2013-304446.

(34) Stansbury, J. W.; Idacavage, M. J. 3D Printing with Polymers: Challenges among Expanding Options and Opportunities. *Dental Materials* **2016**, *32* (1), 54–64. https://doi.org/10.1016/J.DENTAL.2015.09.018.

(35) Silver, A. Five Innovative Ways to Use 3D Printing in the Laboratory. *Nature* **2019**, *565* (7737), 123–124. https://doi.org/10.1038/D41586-018-07853-5.

(36) Bogdan, E.; Michorczyk, P. 3D Printing in Heterogeneous Catalysis—The State of the Art. *Materials* **2020**, *13* (20), 1–23. https://doi.org/10.3390/MA13204534.

(37) Bui, J. C.; Davis, J. T.; Esposito, D. V. 3D-Printed Electrodes for Membraneless Water Electrolysis. *Sustainable Energy & Fuels* **2019**, *4* (1), 213–225. https://doi.org/10.1039/C9SE00710E.

(38) Skalická, B.; Matzick, K.; Komersová, A.; Svoboda, R.; Bartoš, M.; Hromádko, L. 3D-Printed Coating of Extended-Release Matrix Tablets: Effective Tool for Prevention of Alcohol-Induced Dose Dumping Effect. *Pharmaceutics* **2021**, *13* (12). https://doi.org/10.3390/PHARMACEUTICS13122123/S1.

(39) Gusmão, R.; Browne, M. P.; Sofer, Z.; Pumera, M. The Capacitance and Electron Transfer of 3D-Printed Graphene Electrodes Are Dramatically Influenced by the Type of Solvent Used for Pre-Treatment. *Electrochemistry Communications* **2019**, *102*, 83–88. https://doi.org/10.1016/J.ELECOM.2019.04.004.

(40) Tully, J. J.; Meloni, G. N. A Scientist's Guide to Buying a 3D Printer: How to Choose the Right Printer for Your Laboratory. *Analytical Chemistry* **2020**, *92* (22), 14853–14860. https://doi.org/10.1021/ACS.ANALCHEM.0C03299/SUPPL_FILE/AC0C03299_SI_001.PDF.

(41) *Material guide | Prusa Knowledge Base*. https://help.prusa3d.com/category/material-guide_220 (accessed 2022-06-17).

(42) Stansbury, J. W.; Idacavage, M. J. 3D Printing with Polymers: Challenges among Expanding Options and Opportunities. *Dental Materials* **2016**, *32* (1), 54–64. https://doi.org/10.1016/J.DENTAL.2015.09.018.

(43) Ligon, S. C.; Liska, R.; Stampfl, J.; Gurr, M.; Mülhaupt, R. Polymers for 3D Printing and Customized Additive Manufacturing. *Chemical Reviews* **2017**, *117* (15), 10212–10290. https://doi.org/10.1021/ACS.CHEMREV.7B00074.

(44) Mark Editor, J. E. Physical Properties of Polymers Handbook Second Edition.

(45) Dudowicz, J.; Freed, K. F.; Douglas, J. F. The Glass Transition Temperature of Polymer Melts. *Journal of Physical Chemistry B* **2005**, *109* (45), 21285–21292. https://doi.org/10.1021/JP0523266/ASSET/IMAGES/LARGE/JP0523266F00004.JPEG.

(46) Qin, X.; Xia, W.; Sinko, R.; Keten, S. Tuning Glass Transition in Polymer Nanocomposites with Functionalized Cellulose Nanocrystals through Nanoconfinement. *Nano Letters* **2015**, *15* (10), 6738–6744. https://doi.org/10.1021/ACS.NANOLETT.5B02588/ASSET/IMAGES/LARGE/NL-2015-025883_0005.JPEG.

(47) Song, Y.; Ji, X.; Dong, M.; Li, R.; Lin, Y. N.; Wang, H.; Wooley, K. L. Advancing the Development of Highly-Functionalizable Glucose-Based Polycarbonates by Tuning of the Glass Transition Temperature. *J Am Chem Soc* **2018**, *140* (47), 16053–16057. https://doi.org/10.1021/JACS.8B10675/SUPPL_FILE/JA8B10675_SI_001.PDF.

(48) Lotti, N.; Colonna, M.; Fiorini, M.; Finelli, L.; Berti, C. Poly(Ethylene Terephthalate), Modified with Bisphenol S Units, with Increased Glass Transition Temperature. *Journal of Applied Polymer Science* **2013**, *128* (1), 416–423. https://doi.org/10.1002/APP.38165.

(49) Wang, Y. H.; Wang, W. H.; Zhang, Z.; Xu, L.; Li, P. Study of the Glass Transition Temperature and the Mechanical Properties of PET/Modified Silica Nanocomposite by Molecular Dynamics Simulation. *European Polymer Journal* **2016**, *75*, 36–45. https://doi.org/10.1016/J.EURPOLYMJ.2015.11.038.

(50) Liu, W.; Tian, X.; Cui, P.; Li, Y.; Zheng, K.; Yang, Y. Preparation and Characterization of PET/Silica Nanocomposites. *Journal of Applied Polymer Science* **2004**, *91* (2), 1229–1232. https://doi.org/10.1002/APP.13284.

(51) Monemian, S. A.; Goodarzi, V.; Zahedi, P.; Angaji, M. T. PET/Imidazolium-Based OMMT Nanocomposites via in Situ Polymerization: Morphological, Thermal, and Nonisothermal Crystallization Studies. *Advances in Polymer Technology* **2007**, *26* (4), 247–257. https://doi.org/10.1002/ADV.20105.

(52) Ferrannini, E. The Theoretical Bases of Indirect Calorimetry: A Review. *Metabolism*. W.B. Saunders March 1, 1988, pp 287–301. https://doi.org/10.1016/0026-0495(88)90110-2.

(53) Kalichevsky, M. T.; Jaroszkiewicz, E. M.; Ablett, S.; Blanshard, J. M. V.; Lillford, P. J. The Glass Transition of Amylopectin Measured by DSC, DMTA and NMR. *Carbohydrate Polymers* **1992**, *18* (2), 77–88. https://doi.org/10.1016/0144-8617(92)90129-E.

(54) Rieger, J. The Glass Transition Temperature Tg of Polymers—Comparison of the Values from Differential Thermal Analysis (DTA, DSC) and Dynamic Mechanical Measurements (Torsion Pendulum). *Polymer Testing* **2001**, *20* (2), 199–204. https://doi.org/10.1016/S0142-9418(00)00023-4.

(55) Overview of Glass Transition Analysis by Differential Scanning Calorimetry.

(56) Moynihan, C. T.; Easteal, A. J.; Wilder, J.; Tucker, J. Dependence of the Glass Transition Temperature on Heating and Cooling Rate. *Journal of Physical Chemistry* **1974**, *78* (26), 2673–2677. https://doi.org/10.1021/J100619A008/ASSET/J100619A008.FP.PNG_V03.

(57) Polli, H.; Pontes, L.; Araujo, A.; Barros, J.; Fernandes, V. Degradation Behavior and Kinetic Study of ABS Polymer. *Journal of Thermal Analysis and Calorimetry* **2009**, *95* (1), 131–134. https://doi.org/10.1007/S10973-006-7781-1.

(58) *Ultimate 3D Printing Material Properties Table*. https://www.simplify3d.com/support/materials-guide/properties-table/ (accessed 2021-10-25).

(59) Barry, S. T. *Chemistry of Atomic Layer Deposition*; De Gruyter, 2021.

(60) Wilkes, C. E.; Daniels, C. A.; Summers, J. W. PVC Handbook.

(61) M. D. Groner, †; F. H. Fabreguette, †; J. W. Elam, † and; S. M. George*, †,‡. Low-Temperature Al2O3 Atomic Layer Deposition. *Chemistry of Materials* **2004**, *16* (4), 639–645. https://doi.org/10.1021/CM0304546.

(62) Zhang, W.; Wu, A. S.; Sun, J.; Quan, Z.; Gu, B.; Sun, B.; Cotton, C.; Heider, D.; Chou, T. W. Characterization of Residual Stress and Deformation in Additively Manufactured ABS Polymer and Composite Specimens. *Composites Science and Technology* **2017**, *150*, 102–110. https://doi.org/10.1016/J.COMPSCITECH.2017.07.017.

(63) Gong, B.; Peng, Q.; Jur, J. S.; Devine, C. K.; Lee, K.; Parsons, G. N. Sequential Vapor Infiltration of Metal Oxides into Sacrificial Polyester Fibers: Shape

Replication and Controlled Porosity of Microporous/Mesoporous Oxide Monoliths. *Chemistry of Materials* **2011**, *23* (15), 3476–3485. https://doi.org/10.1021/CM200694W.

(64) CreativeTools. *#3DBenchy - The jolly 3D printing torture-test by CreativeTools.se by CreativeTools - Thingiverse*. https://www.thingiverse.com/thing:763622 (accessed 2021-11-03).

(65) Varga, A. C.; Barry, S. T. Modified 3D-Printed Architectures: Effects of Coating by Alumina on Acrylonitrile Butadiene Styrene. *Journal of Vacuum Science & Technology A: Vacuum, Surfaces, and Films* **2022**, *40* (2), 022407. https://doi.org/10.1116/6.0001595.

(66) Skalická, B.; Matzick, K.; Komersová, A.; Svoboda, R.; Bartoš, M.; Hromádko, L. 3D-Printed Coating of Extended-Release Matrix Tablets: Effective Tool for Prevention of Alcohol-Induced Dose Dumping Effect. *Pharmaceutics* **2021**, *13* (12). https://doi.org/10.3390/pharmaceutics13122123.

(67) Hugh O'Connor; J. Bailey, J.; M. Istrate, O.; A. Klusener, P. A.; Rob Watson; Stephen Glover; Francesco Iacoviello; L. Brett, D. J.; R. Shearing, P.; Peter Nockemann. An Open-Source Platform for 3D-Printed Redox Flow Battery Test Cells. *Sustainable Energy & Fuels* **2022**, *6* (6), 1529–1540. https://doi.org/10.1039/D1SE01851E.

(68) Miikkulainen, V.; Leskelä, M.; Ritala, M.; Puurunen, R. L. Crystallinity of Inorganic Films Grown by Atomic Layer Deposition: Overview and General Trends. *Journal of Applied Physics* **2013**, *113* (2). https://doi.org/10.1063/1.4757907.

(69) Leskelä, M.; Ritala, M. Atomic Layer Deposition Chemistry: Recent Developments and Future Challenges. *Angewandte Chemie - International Edition*. John Wiley & Sons, Ltd November 24, 2003, pp 5548–5554. https://doi.org/10.1002/anie.200301652.

(70) Petit, R. R.; Li, J.; Van De Voorde, B.; Van Vlierberghe, S.; Smet, P. F.; Detavernier, C. Atomic Layer Deposition on Polymer Thin Films: On the Role of Precursor

Infiltration and Reactivity. *Cite This: ACS Appl. Mater. Interfaces* **2021**, *13*, 46151–46163. https://doi.org/10.1021/acsami.1c12933.

(71) Sanchez, C.; Belleville, P.; Popall, M.; Nicole, L. Applications of Advanced Hybrid Organic–Inorganic Nanomaterials: From Laboratory to Market. *Chemical Society Reviews* **2011**, *40* (2), 696–753. https://doi.org/10.1039/C0CS00136H.

(72) Lee, M. M.; Teuscher, J.; Miyasaka, T.; Murakami, T. N.; Snaith, H. J. Efficient Hybrid Solar Cells Based on Meso-Superstructured Organometal Halide Perovskites. *Science (1979)* **2012**, *338* (6107), 643–647. https://doi.org/10.1126/SCIENCE.1228604/SUPPL_FILE/LEE.SM.PDF.

(73) Kuppler, R. J.; Timmons, D. J.; Fang, Q. R.; Li, J. R.; Makal, T. A.; Young, M. D.; Yuan, D.; Zhao, D.; Zhuang, W.; Zhou, H. C. Potential Applications of Metal-Organic Frameworks. *Coordination Chemistry Reviews* **2009**, *253* (23–24), 3042–3066. https://doi.org/10.1016/J.CCR.2009.05.019.

(74) Keddie, J. L.; Jones, R. A. L.; Cory, R. A. Size-Dependent Depression of the Glass Transition Temperature in Polymer Films. *EPL (Europhysics Letters)* **1994**, *27* (1), 59. https://doi.org/10.1209/0295-5075/27/1/011.

(75) Forrest, J. A.; Dalnoki-Veress, K.; Stevens, J. R.; Dutcher, J. R. Effect of Free Surfaces on the Glass Transition Temperature of Thin Polymer Films. *Physical Review Letters* **1996**, *77* (10), 2002. https://doi.org/10.1103/PhysRevLett.77.2002.

(76) Turi, E. A. Thermal Characterization of Polymeric Materials. **1981**, 972.

(77) Rahman, M.; Schoot, N. R.; Sadhu, L. K. Glass Transition of ABS in 3D Printing . In *COMSOL Conference*; Boston, 2016.

(78) Gupta, S. S.; Solanki, N.; Serajuddin, A. T. M. Investigation of Thermal and Viscoelastic Properties of Polymers Relevant to Hot Melt Extrusion, IV: Affinisol™ HPMC HME Polymers. *AAPS PharmSciTech* **2016**, *17* (1), 148–157. https://doi.org/10.1208/S12249-015-0426-6/TABLES/3.

(79) Alberts, E.; Ballentine, M.; Barnes, E.; Kennedy, A. Impact of Metal Additives on Particle Emission Profiles from a Fused Filament Fabrication 3D Printer. *Atmospheric Environment* **2021**, *244*, 117956. https://doi.org/10.1016/J.ATMOSENV.2020.117956.

(80) Liang, H.; Zheng, L.; Liao, S. Self-Humidifying Membrane Electrode Assembly Prepared by Adding PVA as Hygroscopic Agent in Anode Catalyst Layer. *International Journal of Hydrogen Energy* **2012**, *37* (17), 12860–12867. https://doi.org/10.1016/J.IJHYDENE.2012.05.083.

(81) Yang, P.; Feng, C.; Liu, Y.; Cheng, T.; Yang, X.; Liu, H.; Liu, K.; Jin Fan, H.; Yang, P.; Liu, Y.; Fan, H. J.; Feng, C.; Cheng, T.; Yang, X.; Liu, H.; Liu, K. Thermal Self-Protection of Zinc-Ion Batteries Enabled by Smart Hygroscopic Hydrogel Electrolytes. *Advanced Energy Materials* **2020**, *10* (48), 2002898. https://doi.org/10.1002/AENM.202002898.

(82) Rathod, V. T.; Kumar, J. S.; Jain, A. Polymer and Ceramic Nanocomposites for Aerospace Applications. *Applied Nanoscience 2017 7:8* **2017**, *7* (8), 519–548. https://doi.org/10.1007/S13204-017-0592-9.

(83) Gouzman, I.; Grossman, E.; Verker, R.; Atar, N.; Bolker, A.; Eliaz, N.; Gouzman, I.; Grossman, E.; Verker, R.; Atar, N.; Bolker, A.; Eliaz, N. Advances in Polyimide-Based Materials for Space Applications. *Advanced Materials* **2019**, *31* (18), 1807738. https://doi.org/10.1002/ADMA.201807738.

# Appendix

**Figure S6.1** Two structures were printed in ABS; an untreated one (left), and one annealed as a pre-treatment and then coated using the same pulse program as used in ABS-B5 (right). Both structures were placed on a stage in a desiccator with ~20 mL of acetone at the bottom. Time is in Hours:Minutes. Video link: https://youtu.be/iPg_9tKs5eE

**Table S6.1** DSC Calculated $T_g$ with averages and standard deviation (SD) for ABS polymer samples. Where run name indicates the number of ALD cycles, U is an uncoated sample and U-PH is an uncoated pre-heated sample to mimic deposition temperatures.

| ABS | | | | | | |
|---|---|---|---|---|---|---|
| **Run Name** | **Tg / ˚C** | | | | **Average** | **SD** |
| **ABS-U** | 103.22 | 102.93 | 103.89 | 103.67 | 103.43 | 0.43 |
| **ABS-U-PH** | 103.20 | 103.25 | 103.22 | 102.91 | 103.15 | 0.14 |
| **ABS-10** | 105.87 | 106.60 | 106.45 | 106.56 | 106.37 | 0.34 |
| **ABS-25** | 106.84 | 107.34 | 107.16 | 106.76 | 107.03 | 0.27 |
| **ABS-40** | 107.92 | 108.26 | 108.13 | | 108.10 | 0.17 |
| **ABS-50** | 111.18 | 110.85 | 111.26 | 109.96 | 110.81 | 0.60 |
| **ABS-75** | 109.45 | 110.20 | 109.93 | 109.69 | 109.82 | 0.32 |
| **ABS-100** | 110.15 | 109.88 | 109.91 | 109.56 | 109.88 | 0.24 |
| **ABS-250** | 109.18 | 109.51 | 109.78 | 109.36 | 109.46 | 0.25 |
| **ABS-500** | 111.92 | 112.85 | 111.77 | 111.87 | 112.10 | 0.50 |

**Table S6.2** DSC Calculated $T_g$ with averages and standard deviation (SD) for PVA polymer samples. Where run name indicates the number of ALD cycles, U is an uncoated sample and U-PH is an uncoated pre-heated sample to mimic deposition temperatures.

| PVA | | | | | | |
|---|---|---|---|---|---|---|
| **Run Name** | **Tg / ˚C** | | | | **Average** | **SD** |
| **PVA-U** | 48.15 | 48.86 | 48.02 | | 48.34 | 0.45 |
| **PVA-U-PH** | 54.56 | 54.70 | 54.53 | | 54.60 | 0.09 |
| **PVA-5** | 81.15 | 81.30 | 82.17 | 80.89 | 81.38 | 0.55 |
| **PVA-10** | 81.01 | 79.80 | 79.87 | 79.81 | 80.12 | 0.59 |
| **PVA-25** | 81.94 | 81.49 | 80.65 | 81.27 | 81.34 | 0.54 |
| **PVA-50** | 80.96 | 80.43 | 80.46 | | 80.62 | 0.30 |
| **PVA-100** | 82.47 | 82.55 | 82.53 | 82.81 | 82.59 | 0.15 |
| **PVA-500** | 81.24 | 81.86 | 81.02 | 82.84 | 81.74 | 0.82 |